Cell Reports

Article

Arabidopsis ATXR2 represses *de novo* shoot organogenesis in the transition from callus to shoot formation

Graphical abstract

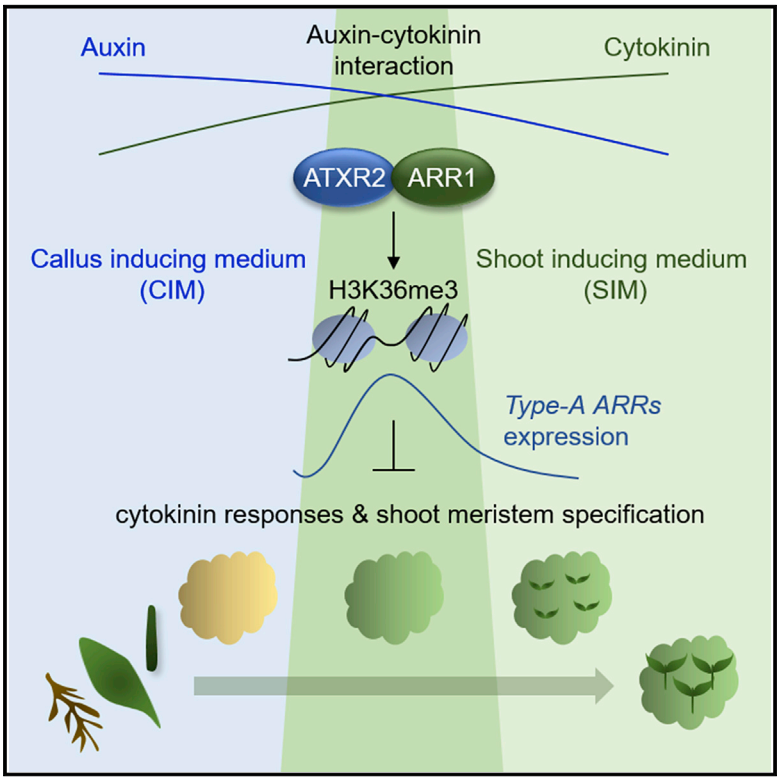

Highlights

- The auxin-cytokinin interaction underlies at early stage of shoot regeneration
- The auxin-inducible ATXR2 transiently interacts with type-B ARR1 on shoot-inducing medium
- The ATXR2-ARR1 complex directly activates type-A *ARR* genes
- The ATXR2/ARR1-type-A ARR module temporally represses cytokinin responses on SIM

Authors

Kyounghee Lee, Ok-Sun Park, Ji Yun Go, ..., Sangsu Bae, Yu Jin Jung, Pil Joon Seo

Correspondence

pjseo1@snu.ac.kr

In brief

Lee et al. demonstrate that the auxin-cytokinin interaction is critical at the early stage of shoot regeneration. The auxin-inducible ATXR2 protein transiently interacts type-B ARR1 protein on SIM, and the ATXR2-ARR1 complex directly activates type-A *ARR* genes to ensure temporal repression of cytokinin responses for proper cell fate transition.

Lee et al., 2021, Cell Reports *37*, 109980
November 9, 2021
https://doi.org/10.1016/j.celrep.2021.109980

CellPress

Cell Reports

CellPress
OPEN ACCESS

Article

Arabidopsis ATXR2 represses *de novo* shoot organogenesis in the transition from callus to shoot formation

Kyounghee Lee,[1,2] Ok-Sun Park,[3] Ji Yun Go,[4] Jihyeon Yu,[5,7] Jun Hee Han,[5] Jungmook Kim,[6] Sangsu Bae,[5] Yu Jin Jung,[4] and Pil Joon Seo[1,2,3,8,*]

[1]Department of Chemistry, Seoul National University, Seoul 08826, Korea
[2]Research Institute of Basic Sciences, Seoul National University, Seoul 08826, Korea
[3]Plant Genomics and Breeding Institute, Seoul National University, Seoul 08826, Korea
[4]Division of Horticultural Biotechnology, Hankyong National University, Anseong 17579, Korea
[5]Department of Chemistry and Research Institute for Convergence of Basic Sciences, Hanyang University, Seoul 04763, Korea
[6]Department of Bioenergy Science and Technology and Department of Integrative Food, Bioscience and Biotechnology, Chonnam National University, Gwangju 61186, Korea
[7]Present address: Division of Life Science, Korea Polar Research Institute, Incheon, 21990, Korea
[8]Lead contact
*Correspondence: pjseo1@snu.ac.kr
https://doi.org/10.1016/j.celrep.2021.109980

SUMMARY

Plants exhibit high regenerative capacity, which is controlled by various genetic factors. Here, we report that *ARABIDOPSIS* TRITHORAX-RELATED 2 (ATXR2) controls *de novo* shoot organogenesis by regulating auxin-cytokinin interaction. The auxin-inducible ATXR2 Trithorax Group (TrxG) protein temporally interacts with the cytokinin-responsive type-B *ARABIDOPSIS* RESPONSE REGULATOR 1 (ARR1) at early stages of shoot regeneration. The ATXR2-ARR1 complex binds to and deposits the H3K36me3 mark in the promoters of a subset of type-A *ARR* genes, *ARR5* and *ARR7*, thus activating their expression. Consequently, the ATXR2/ARR1-type-A ARR module transiently represses cytokinin signaling and thereby *de novo* shoot regeneration. The *atxr2-1* mutant calli exhibit enhanced shoot regeneration with low expression of *ARR5* and *ARR7*, which ultimately upregulates *WUSCHEL* (*WUS*) expression. Thus, ATXR2 regulates cytokinin signaling and prevents premature *WUS* activation to ensure proper cell fate transition, and the auxin-cytokinin interaction underlies the initial specification of shoot meristem in callus.

INTRODUCTION

Plant somatic cells can undergo reprogramming to produce pluripotent callus cells for tissue repair and *de novo* tissue regeneration. A balance between auxin and cytokinin is critical for cell fate reprogramming and *de novo* shoot/root specification (Cheng et al., 2013; Ikeuchi et al., 2013). Explants derived from differentiated plant tissues can be used to generate a pluripotent cell mass, called callus, on auxin-rich callus-inducing medium (CIM) (Cheng et al., 2013). Callus tissues resemble lateral root primordium (LRP) (Atta et al., 2009; Sugimoto et al., 2010); consistently, signaling networks implicated in lateral root initiation significantly overlap with those involved in callus formation (Fan et al., 2012; Sugimoto et al., 2010). For example, protein factors involved in lateral root initiation and LRP establishment, including ABERRANT LATERAL ROOT FORMATION4 (ALF4), AUXIN RESPONSE FACTOR7 (ARF7), ARF19, LATERAL ORGAN BOUNDARIES DOMAIN16 (LBD16), and LBD29, also participate in callus formation (Fan et al., 2012; Sugimoto et al., 2010). Furthermore, key root meristem regulators, including PLETHORA1 (PLT1), PLT2, and WUSCHEL-RELATED HOMEOBOX5 (WOX5), are expressed in pluripotent callus to induce competence for tissue regeneration (Kareem et al., 2015).

Upon acquiring regeneration competence, the pluripotent callus establishes shoot progenitors, thus promoting shoot induction on cytokinin-rich shoot-inducing medium (SIM) (Che et al., 2007; Iwase et al., 2017). The *PLT3*, *PLT5*, and *PLT7* genes, which are induced at early stages of callus formation, contribute to the progression of shoot formation by activating shoot meristem initiation genes, including *CUP-SHAPED COTYLEDON1* (*CUC1*) and *CUC2* (Kareem et al., 2015). The *CUC2*-expressing callus cells continue to form shoot promeristem by regulating the spatial expression of *PIN-FORMED 1* (*PIN1*) and *SHOOT MERISTEMLESS* (*STM*) (Galbiati et al., 2013; Gordon et al., 2007; Kamiuchi et al., 2014). Consistently, the phenotype of the *plt3 plt5 plt7* triple mutant is defective in shoot regeneration because of the failure of CUC2-mediated shoot fate initiation (Kareem et al., 2015). Additionally, the APETALA2 (AP2)/ETHYLENE RESPONSE FACTOR (ERF) transcription factors, ENHANCER OF SHOOT REGENERATION1/DORNROSCHEN

(ESR1/DRN) and ESR2/DRN-LIKE (DRNL), also promote CUC-dependent shoot regeneration (Ikeda et al., 2006; Iwase et al., 2017; Matsuo et al., 2011). In parallel, the cytokinin-responsive type-B ARR proteins, including ARR1, ARR10, and ARR12, are progressively expressed during *de novo* shoot organogenesis and directly activate *WUS* expression in the high-cytokinin response domains to specify shoot meristem, promoting *de novo* shoot regeneration (Zhang et al., 2017). It is supported by the impaired shoot regeneration phenotype of the *arr1 arr12* double mutant, which is rescued by the ectopic expression of *WUS* (Zhang et al., 2017).

Notably, *de novo* shoot regeneration is further balanced by cell division control. Shoot regeneration in callus requires extensive cell division (Liu et al., 2018), which enables cells to regenerate stem cell niche and diverse organs. Application of cell cycle inhibitors to SIM significantly impairs *de novo* organogenesis in *Arabidopsis* (Che et al., 2007). The cyclin-dependent kinase (CDK) inhibitor genes *ICK*s/*KRP*s play a negative role in shoot regeneration (Liu et al., 2016). Genetic defects in *ICKs*/*KRPs* stimulate the E2Fa pathway and cell proliferation, thus promoting plant regeneration (Cheng et al., 2015; Liu et al., 2016). Similarly, type-A ARR proteins, negative regulators of cytokinin signaling and cell division, are also implicated in the suppression of *de novo* shoot organogenesis in callus (Buechel et al., 2010). Overexpression of *ARR7* and *ARR15* suppresses shoot regeneration, whereas loss-of-function mutations in several type-A *ARR*s promote *de novo* shoot organogenesis (Buechel et al., 2010). Inhibition of cell proliferation is particularly important for proper cell fate transition at the initial stage of shoot stem cell specification in callus, as a temporal cell division cease is frequently observed upon transferring calli from CIM to SIM (Tamaki et al., 2009; Tian et al., 2018). The balanced cell proliferation at the cell fate transition is potentially linked to auxin-cytokinin interactions, although the underlying molecular mechanisms are largely unknown (Bustillo-Avendaño et al., 2018).

Here, we report that the auxin-activated ATXR2 protein interacts with cytokinin-responsive ARR1 and represses *de novo* shoot regeneration on SIM by activating type-A *ARR5* and *ARR7*. ATXR2 binds to and catalyzes H3K36me3 deposition at *ARR5* and *ARR7* promoters in an ARR1-dependent manner. ATXR2 exhibits an evolutionarily conserved function across many plant species, and is crucial for balancing cell division to ensure proper cell fate transition during *de novo* shoot regeneration (Bustillo-Avendaño et al., 2018).

RESULTS

atxr2-1 mutant exhibits enhanced *de novo* shoot organogenesis ability

ATXR2 is known to participate in auxin-dependent callus formation, along with ARF7 and ARF19 (Lee et al., 2017). As callus formation is usually followed by cytokinin-triggered *de novo* shoot organogenesis in conventional *in vitro* tissue culture methods, we were curious to know the impact of ATXR2 on shoot regeneration. The importance of this question was further substantiated by the observation that *ATXR2* was expressed in upper regions of *Arabidopsis* roots (Figure S1A), where cytokinin-controlled cell division is relevant (Dello Ioio et al., 2008; Moubayidin et al., 2009; Salvi et al., 2020).

Thus, we first examined the shoot regeneration capacity of the *atxr2*-null mutant *atxr2-1*. Leaf explants were pre-incubated on CIM for 6 days and then transferred onto SIM. The regenerated leaves were counted to estimate the ability of the *atxr2-1* mutant to undergo *de novo* shoot organogenesis from callus. A 2.5-fold increase in shoot formation was observed in *atxr2-1* compared with the wild-type (Figures 1A and 1B). Similar results were obtained using hypocotyl and root explants (Figures 1A and 1B), indicating that ATXR2 regulates *de novo* shoot regeneration, regardless of the origin of explants.

However, the function of ATXR2 in shoot regeneration was independent of ARF7 and ARF19. The *arf7-1arf19-2* double mutant showed reduced shoot regeneration (Figures S1B and S1C), unlike the *atxr2-1* mutant (Figures 1A and 1B), which suggests that ATXR2 has a different mode of action during callus formation and *de novo* shoot regeneration.

Consistent with the negative role of *ATXR2* in shoot regeneration, the expression of *ATXR2* increased over time during callus proliferation on auxin-rich CIM but declined after incubation on cytokinin-rich SIM (Figures 1C and 1D). At early stages of shoot regeneration, *ATXR2* was expressed mainly in the middle regions of callus (Figure S1D), which might be pluripotent regions for subsequent tissue regeneration. The control of *ATXR2* expression was likely attributable to hormones in culture media. Exogenous auxin treatment induced *ATXR2* expression, whereas cytokinin treatment repressed *ATXR2* in seedlings (Figure 1E). Meanwhile, the ATXR2 function was independent of natural wounding. Expression of *ATXR2* was unaffected by wounding (Figure 1E), and the enhanced shoot formation in *atxr2-1* was not observed in shoot-removed seedlings on hormone-free medium (Figure S1E). These results imply that the hormone-regulated *ATXR2* gene suppresses *de novo* shoot organogenesis during a two-step plant regeneration process that requires control of hormone signaling.

ATXR2 stimulates the expression of *ARR5* and *ARR7*

Next, we investigated the molecular components regulated by the ATXR2 protein during *de novo* shoot organogenesis. Given that the enhanced shoot regeneration of *atxr2-1* mutant was more exaggerated on low-cytokinin SIM (Figures S2A and S2B), we examined the transcript levels of genes involved in cytokinin metabolism and signaling, such as *ISOPENTENYLTRANSFERASE7* (*IPT7*), *ARABIDOPSIS HISTIDINE KINASE2* (*AHK2*), *ARABIDOPSIS HISTIDINE PHOSPHOTRANSFER PROTEIN6* (*AHP6*), type-B *ARR*s (*ARR1* and *ARR12*), and type-A *ARR*s (*ARR5*, *ARR6*, *ARR7*, and *ARR15*). Wild-type and *atxr2-1* mutant calli were harvested at 2 days after incubation on SIM (DAS), when *ATXR2* expression was maintained at high level on SIM (Figure 1C). Quantitative real-time RT-PCR (qRT-PCR) analysis showed that the expression of type-A *ARR* genes *ARR5* and *ARR7* was lower in *atxr2-1* mutant calli than in wild-type calli, whereas the expression of other genes was either unaffected or increased by the *atxr2* mutation (Figure 2A), suggesting an altered cytokinin signaling homeostasis in *axtr2-1*. As ATXR2 is a transcriptional coactivator, we put more focus on *ARR5* and *ARR7*. It was also noteworthy that high-order mutants

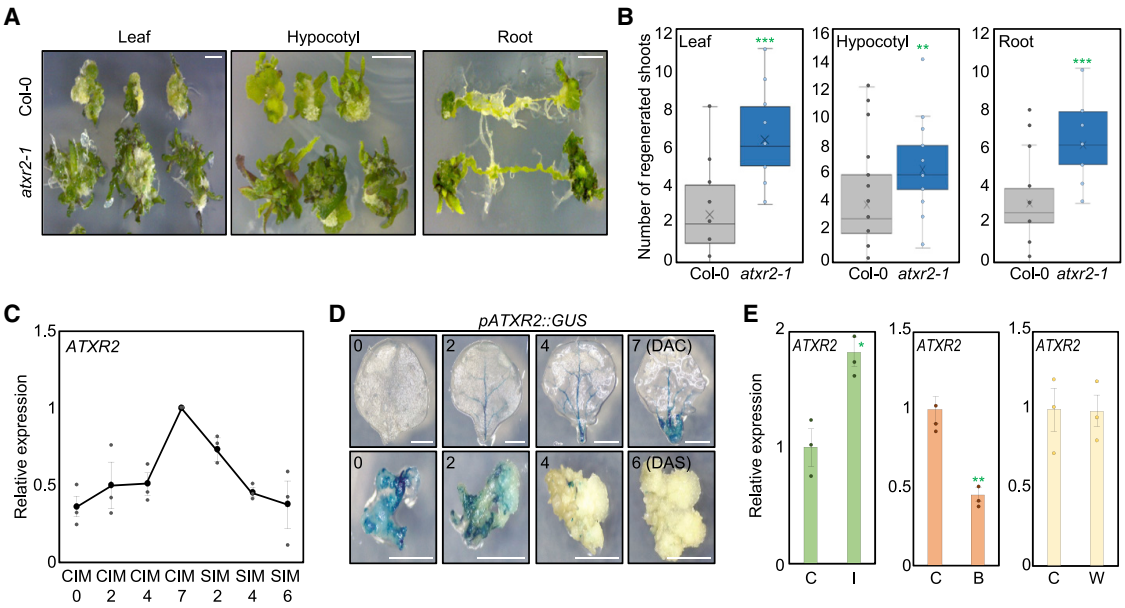

Figure 1. ATXR2 inhibits *de novo* shoot regeneration

(A) *De novo* shoot regeneration from leaf, hypocotyl, and root explants. Calli pre-incubated on callus-inducing medium (CIM) for 6 days were transferred to shoot-inducing medium (SIM) to induce *de novo* shoot regeneration. The SIM plates were incubated under continuous light for 2 weeks (for leaf explants) and 11 days (for hypocotyl and root explants) and photographed. Scale bars, 5 mm.

(B) Number of shoots regenerated from calli. Data represent mean ± SEM of three biological replicates. Statistically significant differences were determined using Student's t test (**$p < 0.01$ and ***$p < 0.001$).

(C) Quantitative real-time RT-PCR (qRT-PCR) analysis of *ATXR2* expression in wild-type leaf explants cultured on CIM and SIM. The *eIF4a* gene (At3g13920) was used as an internal control. Data represent mean ± SEM of three biological replicates.

(D) *ATXR2* promoter activity in *pATXR2::GUS* transgenic leaf explants cultured on CIM and SIM. DAC, days after incubation on CIM; DAS, days after incubation on SIM. Scale bars, 1 mm.

(E) Effects of auxin, cytokinin, and wounding on *ATXR2* expression. In the hormone treatment, 2-week-old seedlings grown under long days (LDs) were transferred to liquid MS medium supplemented with 1 μM IAA (I) or 1 μM BAP (B) and incubated for 24 h. In the wounding (W) treatment, third and fourth leaves of 2-week-old seedlings were excised and placed on hormone-free MS medium for 24 h. Transcript accumulation was analyzed by qRT-PCR. Data represent mean ± SEM of three biological replicates. Statistically significant differences were determined using Student's t test (*$p < 0.05$ and **$p < 0.01$). C, control.

of type-A *ARR* genes exhibited increased *de novo* shoot regeneration (Buechel et al., 2010), similar to *atxr2-1* mutant. The expression of type-A *ARRs* was also reduced in *atxr2* mutant calli derived from other tissue explants (Figure S2C), consistent with the shoot regeneration phenotypes (Figures 1A and 1B).

Being a chromatin modifier, ATXR2 was expected to bind to and modify cognate regions in target gene promoters to regulate gene expression. Therefore, we performed chromatin immunoprecipitation followed by quantitative PCR (ChIP-qPCR) to determine whether ATXR2 can bind to the promoters of genes whose expression was affected by ATXR2 (Figure 2A). ChIP-qPCR analysis using an anti-MYC antibody revealed that ATXR2 selectively binds to the promoters of *ARR5* and *ARR7* but not to those of *ARR1* and *ARR12* (Figures 2B and 2C; Figures S2D and S2E). In addition, the binding of ATXR2 to *ARR5* and *ARR7* promoters was observed only on SIM and not on CIM (Figure S2F). Moreover, the promoter of another type-A *ARR6* gene, whose expression was unaffected by ATXR2 (Figure 2A), was not bound by ATXR2 (Figures S2G and S2H).

We generated transgenic plants expressing ATXR2 fused to the steroid-binding domain of the glucocorticoid receptor (GR) (35S:*ATXR2-GR*). In the presence of the synthetic steroid hormone dexamethasone (DEX), which induces the nuclear targeting of ATXR2-GR fusion proteins and the expression of target genes (Yamaguchi et al., 2015), the expression of *ARR5* and *ARR7* was increased within 4 h, while that of type-B *ARRs* was unaffected (Figure 2D). Next, we performed transient gene expression assays. The reporter plasmid carrying *ARR5* or *ARR7* promoter fused to the 35S minimal promoter was co-transfected with the effector construct expressing the *ATXR2* gene into *Arabidopsis* protoplasts (Figure 2E). Co-expression of these constructs induced a 3- to 5-fold increase in GUS activity, compared with vector control (Figure 2F), indicating that ATXR2 upregulates the expression of type-A *ARR*s.

Notably, the regulation of type-A *ARR*s by ATXR2 was apparent at the early stages of shoot regeneration, when the *ATXR2* transcript level was relatively high (Figure 1C). The accumulation of *ARR5* and *ARR7* transcripts was transiently increased in wild-type calli at 2 DAS, but the transient expression of *ARR5* and *ARR7* was impaired in *atxr2-1* mutant calli (Figure 2G). Furthermore, ATXR2-mediated regulation of type-A *ARR*s was not observed during callus formation (Figure S3A). DEX treatment of 35S:*ATXR2-GR* plants on CIM also failed to promote the expression of *ARR5* and *ARR7* (Figure S3B), further

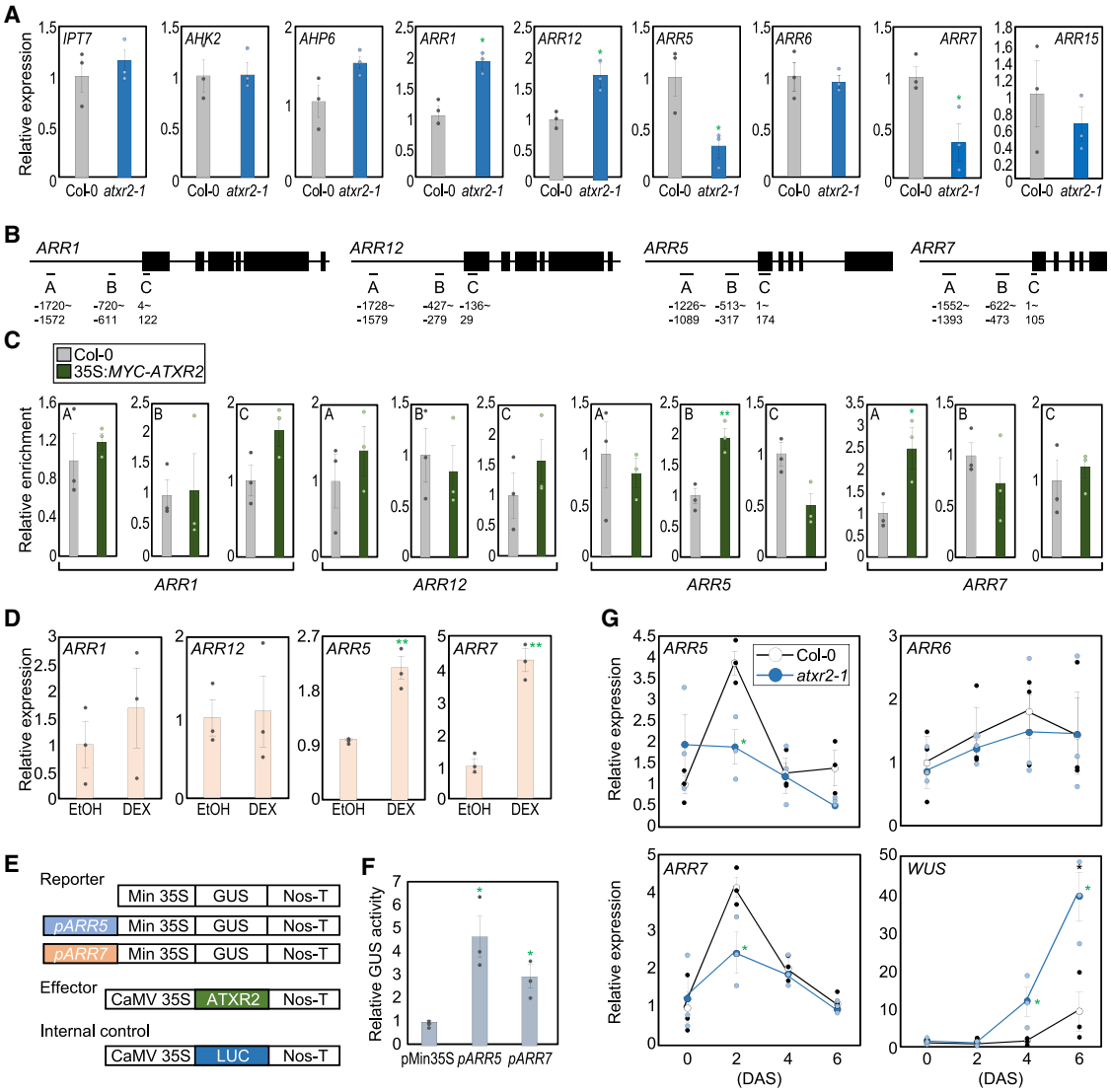

Figure 2. ATXR2 directly regulates the expression of *type-A ARR* genes *ARR5* and *ARR7*

(A) Expression profiling of genes involved in cytokinin metabolism and signaling. Leaf explants derived from the third and fourth leaves of 2-week-old plants were incubated on CIM for 7 days and subsequently on SIM for 2 days. Whole-callus tissues were selectively harvested for gene expression analysis. Transcript accumulation was analyzed by qRT-PCR. The *eIF4a* gene (At3g13920) was used as an internal control. Data represent mean ± SEM of three biological replicates. Asterisks indicate statistically significant differences between wild-type and mutant calli (*$p < 0.05$).

(B) Promoter analysis of *ARR1*, *ARR12*, *ARR5*, and *ARR7* genes. Black lines above the labels indicate regions amplified by quantitative PCR (qPCR) following chromatin immunoprecipitation (ChIP). Black boxes indicate exons.

(C) ChIP assays. Enrichment of precipitated DNA was analyzed using ChIP-qPCR. Values for control plants were set to 1 after normalization against *eIF4a*. Data are mean ± SEM of three biological replicates. Statistically significant differences were determined using Student's t test (*$p < 0.05$ and **$p < 0.01$).

(D) Analysis of changes in the expression of *ARR1*, *ARR12*, *ARR5*, and *ARR7* after dexamethasone (DEX) treatment. Leaf explants derived from the third and fourth leaves of 2-week-old 35S:*ATXR2-GR* transgenic plants were incubated on CIM for 7 days and subsequently on SIM for 4 days. The calli were treated with 10 μM DEX or ethanol (EtOH) for 4 h. Data represent mean ± SEM of three biological replicates. Asterisks indicate statistically significant differences between wild-type and mutant calli (**$p < 0.01$).

(E and F) Transient expression assays. The *ARR5* and *ARR7* promoters were cloned into the reporter plasmid (E), which were transiently co-expressed with the effector constructs into *Arabidopsis* protoplasts, followed by the quantification of GUS activities (F). *Luciferase* gene expression was used to normalize the GUS activities. The normalized values in control protoplasts were set to 1 and represented as relative activation. Data represent mean ± SEM of three biological replicates. Statistically significant differences were determined using Student's t test (*$p < 0.05$).

(G) Expression of *ARR5*, *ARR6*, *ARR7*, and *WUS*. Leaf explants derived from the third and fourth leaves of 2-week-old plants were incubated on CIM for 7 days and subsequently on SIM for up to 6 days. Data represent mean ± SEM of three biological replicates. Asterisks indicate statistically significant differences between wild-type and mutant calli (*$p < 0.05$).

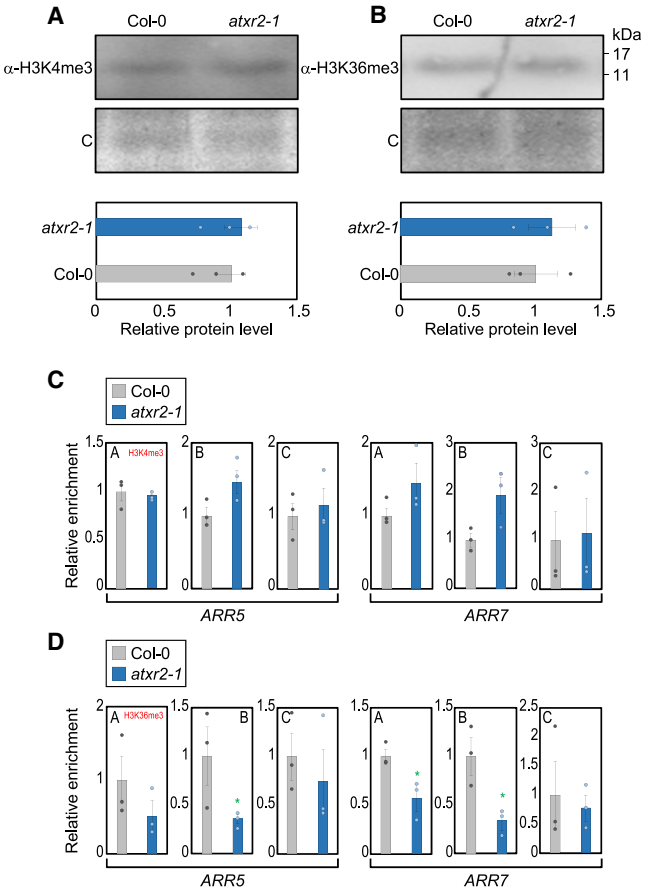

Figure 3. ATXR2 catalyzes H3K36me3 deposition at *ARR5* and *ARR7* loci during shoot regeneration

(A and B) Global accumulation of H3K4me3 (A) and H3K36me3 (B). Bands from three independent blots were quantified (bottom). Data are mean ± SEM of three biological replicates. C, Coomassie blue-stained gel as a loading control.

(C and D) Local accumulation of H3K4me3 (C) and H3K36me3 (D) at *ARR5* and *ARR7* loci. Enrichment of H3K4me3 and H3K36me3 marks at *ARR5* and *ARR7* loci was analyzed using ChIP-qPCR using anti-H3K4me3 and anti-H3K36me3 antibodies, respectively. Data are mean ± SEM of three biological replicates. Statistically significant differences were determined using Student's t test (*$p < 0.05$).

In (A)–(D), leaf explants derived from the third and fourth leaves of 2-week-old plants were incubated on CIM for 6 days and subsequently on SIM for 2 days.

supporting the notion that ATXR2 performs distinct functions during callus formation and *de novo* shoot regeneration (see Discussion). Together, these results indicate that ATXR2 binds to the *ARR5* and *ARR7* promoters to activate their expression and inhibit shoot regeneration at early stages of *de novo* shoot organogenesis on SIM.

ATXR2 deposits the H3K36me3 mark at *ARR5* and *ARR7* loci

The ATXR2 TrxG protein is known to catalyze H3K4me3 and H3K36me3 deposition at its target sites to activate the expression of neighboring genes (Baumbusch et al., 2001; Lee et al., 2017). Thus, we first tested the global accumulation of H3K4me3 and H3K36me3 in calli incubated on SIM. However, no discernable changes were detected in the levels of both methylation marks between wild-type and *atxr2-1* mutant calli (Figures 3A and 3B).

We then examined histone modifications in local chromatin regions bound by ATXR2. There was no difference detected between the wild-type and *atxr2-1* mutant calli in the accumulation of H3K4me3 at *ARR5* and *ARR7* loci at 2 DAS (Figure 3C). However, ChIP-qPCR analysis using anti-H3K36me3 antibody revealed that the level of H3K36me3 mark at *ARR5* and *ARR7* loci was significantly lower in *atxr2-1* mutant calli than in wild-type calli, indicating that H3K36me3 modification occurred at regions nearby the ATXR2-binding sites (Figures 2B, 2C, and 3D). Moreover, the H3K36me3 modification occurred transiently at 2 DAS in an ATXR2-dependent manner (Figures S3C and S3D). These results indicate that ATXR2 catalyzes H3K36me3 deposition locally at the *ARR5* and *ARR7* loci to promote their expression during *de novo* shoot regeneration.

ATXR2 interacts with ARR1

The binding of chromatin modifiers to target sites is usually dependent on DNA-associated transcription factors (Hung et al., 2018; Lee and Seo, 2019; Liu et al., 2013; Ryu et al., 2014). ATXR2 does not require ARFs to perform its function in *de novo* shoot regeneration (Figures S1B and S1C). In addition, ATXR2-mediated regulation of *ARR5* and *ARR7* was relevant only at the early stages of shoot regeneration on SIM (Figure 2G), but not during callus formation (Figures S2F, S3A, and S3B), suggesting that cytokinin signaling factors are required for the ATXR2 function. We hypothesized that type-B ARRs might be plausible candidates, which act upstream of type-A *ARR*s (Xie et al., 2018). We thus examined the expression of *ARR5* and *ARR7* in several *type-B arr* mutant calli. Interestingly, the expression of both *ARR5* and *ARR7* was specifically downregulated in *arr1-3*, but the other *type-B arr* mutants had a limited impact in regulating both *ARR5* and *ARR7* expression (Figure 4A).

To support our results, we conducted yeast two-hybrid (Y2H) assays and validated the physical interactions between ATXR2 and type-B ARRs by the co-expression of GAL4 DNA-binding domain (BD)-ATXR2 and GAL4 activation domain (AD)-ARR fusion proteins. Yeast cell growth on selective medium revealed that ATXR2 interacts specifically with ARR1 (Figure 4B), and this interaction was mediated by the receiver domain of ARR1 (Figures S4A and S4B).

To verify the interaction between ATXR2 and ARR1 *in vivo*, we conducted bimolecular fluorescence complementation (BiFC) assays using *Arabidopsis* protoplasts. The *ATXR2* coding region was fused in-frame to the N-terminal half of the yellow fluorescent protein (nYFP), and the *ARR1* gene was fused in-frame to the C-terminal half of YFP (cYFP). The *ATXR2-nYFP* and *ARR1-cYFP* fusion constructs were then transiently co-expressed in *Arabidopsis* protoplasts. YFP signal was detected exclusively in the nucleus of cells co-expressing both constructs (Figure 4C), whereas co-expression of either construct with an empty vector did not produce visible fluorescence signal (Figure 4C).

The ATXR2-ARR1 interaction was further verified by coimmunoprecipitation (co-IP). We crossed the 35S:*ATXR2-GFP* transgenic plants with 35S:*ARR1-MYC* transgenic plants and

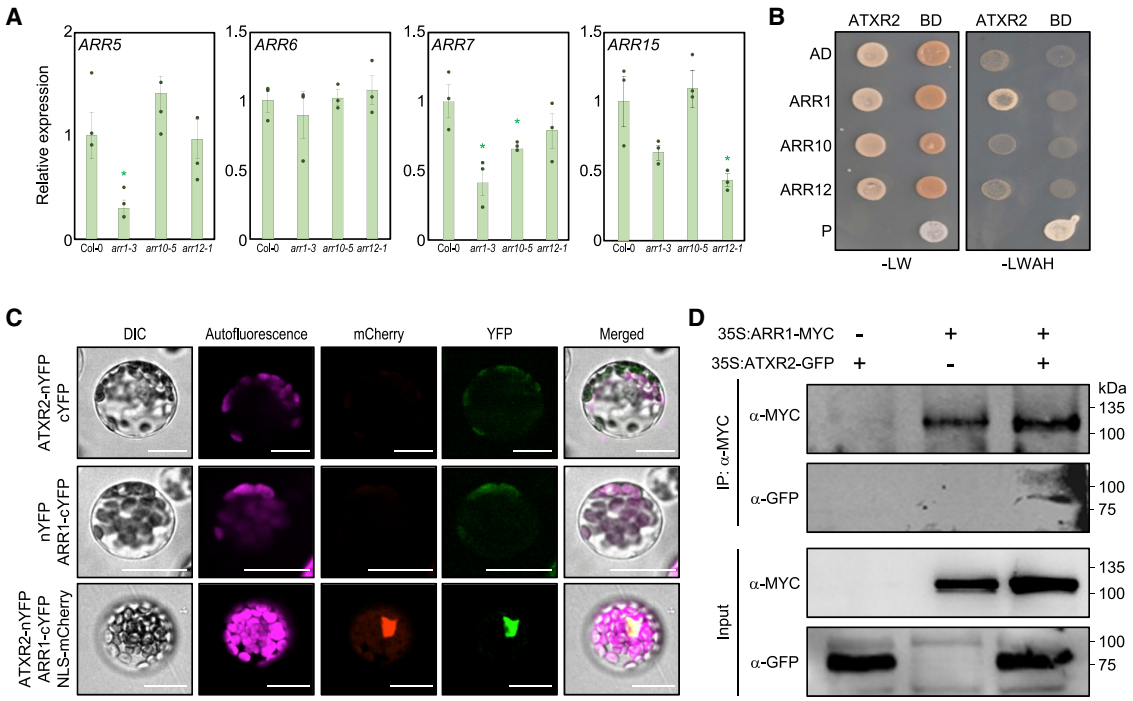

Figure 4. ATXR2 physically interacts with ARR1

(A) Expression analysis of type-A *ARR*s in *arr1-3*, *arr10-5*, and *arr12-1* mutants. Leaf explants derived from the third and fourth leaves of 2-week-old plants were incubated on CIM for 7 days and subsequently on SIM for 4 days. Data represent mean ± SEM of three biological replicates. Asterisks indicate statistically significant differences between wild-type and mutant calli (*$p < 0.05$).

(B) Yeast two-hybrid (Y2H) assays using ATXR2 fused to the GAL4 DNA-binding domain (BD) and ARR1, ARR10, and ARR12 receiver domains fused to the GAL4 transcriptional activation domain (AD). Full-length GAL4 was used as a positive control (P). LW, selection medium lacking leucine and tryptophan; LWAH, selection medium lacking leucine, tryptophan, adenine, and histidine.

(C) Bimolecular fluorescence complementation (BiFC) assays. Partial yellow fluorescent protein (YFP) fusion constructs containing either ATXR2 or ARR1 were transiently co-expressed in *Arabidopsis* protoplasts. The NLS-mCherry construct was used as a nuclear localization marker. Scale bars, 20 μm.

(D) Coimmunoprecipitation (co-IP) assays. Two-week-old 35S:*ATXR2-GFP* × 35S:*ARR1-MYC* transgenic plants were used for co-IP assays. Epitope-tagged proteins were detected immunologically using anti-GFP and anti-MYC antibodies. IP, immunoprecipitation.

performed co-IP assays using anti-MYC antibody. Immunoblot analysis with anti-GFP antibody revealed that ATXR2 interacts with ARR1 in *Arabidopsis* (Figure 4D), indicating that ATXR2 is recruited specifically by ARR1 to regulate the expression of type-A *ARR*s during cell fate transition on SIM.

ARR1 facilitates H3K36me3-dependent activation of *ARR5* and *ARR7*

Given that ATXR2 represses shoot regeneration, we asked whether ARR1 also negatively regulates shoot regeneration. Unlike other type-B ARR proteins, ARR1 repressed shoot regeneration (Figures 5A and 5B), consistent with previous reports (Liu et al., 2020b). The shoot regeneration capacity was enhanced in the *arr1-3* mutant but decreased in *arr12-1* (Figures 5A and 5B). The increase in *arr1-3* shoot regeneration was possibly attributable to the low expression of *ARR5* and *ARR7* (Figure 5C), similar to the *atxr2-1* mutant (Figure 2G).

Consistent with the physical interaction between ARR1 and ATXR2, it was shown that type-B ARRs directly bind to type-A *ARR* loci to activate their expression (Xie et al., 2018; Zubo et al., 2017). We confirmed this finding by showing that ARR1 directly binds to *ARR5* and *ARR7* promoters (Figure S4C). Furthermore, consistent with the observation that ATXR2 induced H3K36me3 deposition (Figure 3D), the accumulation of H3K36me3 at *ARR5* and *ARR7* loci was lower in *arr1-3* mutant calli than in wild-type calli (Figure 5D).

Next, we examined whether the binding of ATXR2 to the *ARR5* and *ARR7* promoters is dependent on ARR1. A 35S:*MYC-ATXR2* transgenic plant was crossed with the *arr1-3* mutant, in which the level of ATXR2 protein was similar to that in 35S:*MYC-ATXR2* (Figure S4D). The resultant 35S:*MYC-ATXR2* × *arr1-3* transgenic plants were used for ChIP-qPCR analysis using anti-MYC antibody. The results showed that although ATXR2 was associated with *ARR5* and *ARR7* promoters in the wild-type, its binding to these promoters was substantially diminished in the *arr1-3* mutant (Figure 5E). Furthermore, transient expression assays using *Arabidopsis* protoplasts showed that the expression of *ATXR2* increased the promoter activity of type-A *ARR*s in wild-type protoplasts; however, the activation of type-A *ARR*s by ATXR2 was significantly compromised in *arr1-3* mutant protoplasts (Figures 5F and 5G). Control assays confirmed that the type-A *ARR* regulation by ATXR2 was dependent on ARR1, but

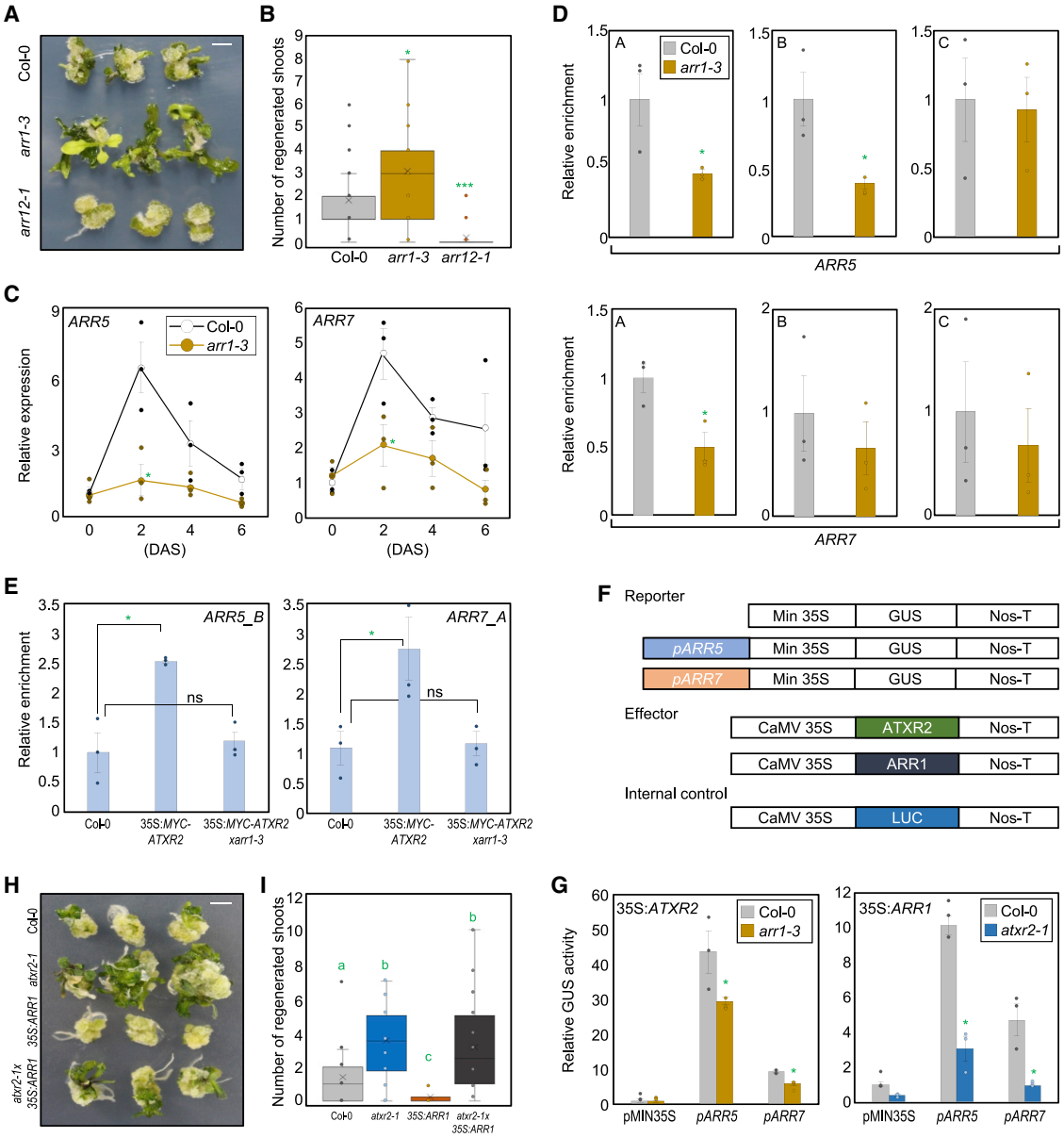

Figure 5. ATXR2 depends on ARR1 for the regulation of *ARR5* and *ARR7* expression

(A) Shoot regeneration of the *arr1-3* mutant. Calli pre-incubated on CIM for 7 days were transferred to SIM to induce *de novo* shoot regeneration. SIM plates were incubated under continuous light for 2 weeks and photographed. Scale bars, 5 mm.

(B) Number of shoots regenerated from calli at 2 weeks after incubation on SIM. Data represent mean ± SEM of three biological replicates. Statistically significant differences were determined using Student's t test (*$p < 0.05$ and ***$p < 0.001$).

(C) *ARR5* and *ARR7* expression during incubation on SIM. Leaf explants derived from the third and fourth leaves of 2-week-old plants were incubated on CIM for 7 days and subsequently on SIM for up to 6 days. Data represent mean ± SEM of three biological replicates. Asterisks indicate statistically significant differences between wild-type and mutant calli (*$p < 0.05$). DAS, days after incubation on SIM.

(D) H3K36me3 accumulation at *ARR5* and *ARR7* loci in *arr1-3* calli. Enrichment of precipitated DNA was analyzed using ChIP-qPCR. Data are mean ± SEM of three biological replicates (*$p < 0.05$, Student's t test).

(E) Impairment of ATXR2 binding to *ARR5* and *ARR7* promoters in the *arr1-3* mutant. Enrichment of promoter regions was analyzed using ChIP-qPCR using anti-MYC antibody. Data indicate mean ± SEM of three biological replicates (*$p < 0.05$, Student's t test). ns, not significant.

(F and G) Transient expression assays. The *ARR5* and *ARR7* promoters were cloned into the reporter plasmid (F) and transiently co-expressed with the effector constructs into *Arabidopsis* protoplasts, followed by the quantification of GUS activities (G). *Luciferase* gene expression was used to normalize the GUS activities. The normalized values in control protoplasts were set to 1 and represented as relative activation. Data indicate mean ± SEM of three biological replicates. Statistically significant differences were determined using Student's t test (*$p < 0.05$).

(legend continued on next page)

not ARF transcription factors (Figures S5A and S5B), indicating that ATXR2 requires the ARR1 protein for binding to *ARR5* and *ARR7* loci to facilitate H3K36me3-dependent gene activation.

Notably, the type-B ARR1 protein also requires ATXR2 for substantially increasing the expression of type-*A ARR* genes. The increase in H3K36me3 level due to the ectopic expression of *ARR1* was also reduced in *atxr2-1* mutant protoplasts (Figure S5C). In addition, transient expression assays also showed that the expression of *ARR1* increased the transcription of type-A *ARR*s in wild-type protoplasts; however, the activation of type-A *ARR*s was significantly compromised in *atxr2-1* mutant protoplasts (Figures 5F and 5G). To confirm the genetic relationship between *ATXR2* and *ARR1*, we crossed *atxr2-1* mutant with 35S:*ARR1* transgenic plants and examined the shoot regeneration capacity. The *atxr2-1* × 35S:*ARR1* calli displayed enhanced shoot regeneration, comparable with *atxr2-1* mutant (Figures 5H and 5I), which indicates that repression of shoot regeneration by ARR1 requires ATXR2. Together, these results demonstrate that ATXR2 and ARR1 are interdependent in the control of *de novo* shoot organogenesis.

ATXR2 acts upstream of type-A ARRs

Accumulating evidence led us to speculate that ATXR2 directly binds to and regulates type-A *ARR* genes. To determine the genetic hierarchy between ATXR2 and type-A ARRs in the *de novo* shoot organogenesis, we crossed the *atxr2-1* mutant with 35S:*ARR7* transgenic plants. The parental genotypes showed obvious differences in shoot regeneration rate; the shoot regeneration capability was high in the *atxr2-1* mutant (Figures 1A and 1B), but low in 35S:*ARR7* transgenic calli (Figures S6A–S6C). The resulting *atxr2-1* × 35S:*ARR7* plants displayed reduced shoot regeneration capability, similar to 35S:*ARR7* transgenic plants (Figures 6A and 6B), indicating that type-A ARRs are epistatic to ATXR2.

The cytokinin-inducible WUS transcription factor plays a crucial role in promoting shoot regeneration (Gordon et al., 2009; Zhang et al., 2017). As type-A ARRs negatively regulate cytokinin signaling (To et al., 2007), we speculated that ATXR2 suppresses *WUS* expression by repressing cytokinin signaling. Indeed, *WUS* expression was higher in *atxr2-1* mutant calli than in wild-type calli on SIM (Figure 6C), consistent with the enhanced shoot regeneration capacity of *atxr2-1*. Moreover, WUS was also epistatic to type-A ARRs (Figures 6D and 6E).

Overall, *ATXR2* expression was detected mainly on CIM but gradually declined on SIM. In contrast, the expression of type-B *ARR*s increased upon incubation on SIM (Figure S6D) (Liu et al., 2020b). Thus, ATXR2 transiently interacts with ARR1 at the initial stages of shoot regeneration (2 DAS). Although the ARR1-ATXR2 complex action was temporally accomplished, it plays an important role in determining the overall shoot regeneration capability. Our data show that the ATXR2-ARR1 complex positively regulates type-A *ARR*s, including *ARR5* and *ARR7*, by binding to their promoter regions and depositing the H3K36me3 mark, and the ATXR2-ARR1-ARR5/7 module ultimately balances *WUS* expression and ensures proper *de novo* shoot regeneration (Figure 6F).

Role of ATXR2 in *de novo* shoot organogenesis is conserved in rice

To determine whether the function of ATXR2 in *de novo* shoot organogenesis is conserved in monocots, we identified the *Arabidopsis ATXR2* homolog in rice (*Oryza sativa*) and examined its role in shoot regeneration. A single copy of the *OsATXR2* gene was identified in the rice genome (Os04 g0629100). To determine the function of *OsATXR2* in shoot regeneration of rice calli, we used CRISPR-Cas9 technology. Two independent single guide RNAs (sgRNAs) complementary to sequences in rice *OsATXR2*, with low homologies to other genomic regions, were designed using the Cas-OFFinder and Cas-Designer programs (http://www.rgenome.net/) (Bae et al., 2014; Kim et al., 2017; Liu et al., 2020a) (Figure 7A). Each sgRNA was individually cloned into a CRISPR-Cas9 vector (Lu et al., 2017; Tomlinson et al., 2019), and the resulting recombinant plasmids were transformed into rice. Genomic DNA was isolated from shoots regenerated from genome-edited calli, and targeted mutagenesis was confirmed by targeted deep-sequencing analysis (Figure 7B).

Two independent homozygous genome-edited lines, each carrying a 1 bp insertion or 7 bp deletion at the target site, were established and used to analyze the rate of *de novo* shoot regeneration. Although the wild-type callus produced a first *de novo* regenerated shoot in approximately 14 DAS, genome-edited *atxr2* mutant rice calli produced a shoot within 10 DAS (Figure 7C). The number of regenerated shoots was also significantly increased in *atxr2* mutant lines compared with the wild-type at 14 DAS (Figure 7D). Taken together, these results indicate that the function of ATXR2 in *de novo* shoot regeneration is evolutionarily conserved in plants (Figure 7E).

DISCUSSION

Multiple epigenetic layers of plant regeneration regulation

Cell fate transition is regulated mainly by chromatin configuration. Consistently, plant regeneration involves genome-wide chromatin modifications, such as DNA methylation, H3 acetylation, and H3K4me3 and H3K27me3 deposition (Chen et al., 2015; He et al., 2012; Kim et al., 2018; Li et al., 2011). Accordingly, many chromatin modifiers play crucial roles in plant regeneration. In differentiated tissues, the POLYCOMB REPRESSIVE COMPLEX2 (PRC2) catalyzes H3K27me3 modification and maintains the transcriptional repression of key reprogramming factors, including *LEAFY COTYLEDON2* (*LEC2*), *BABY BOOM* (*BBM*), *WOUND-INDUCED DEDIFFERENTIATION3* (*WIND3*), *WOX11*, *WOX5*, *WUS*, and *STM* (He et al., 2012; Ikeuchi et al., 2015; Lafos et al., 2011; Liu et al., 2014; Liu et al., 2011). Mutations in genes encoding PRC2 components result in

(H and I) *De novo* shoot regeneration of *atxr2-1* × *35S:ARR1* calli. Calli pre-incubated on CIM for 7 days were used to induce shoot regeneration on SIM ($n > 20$). SIM plates were incubated under continuous light for 26 days and photographed (H). Scale bars, 5 mm. The number of regenerated leaves derived from calli was counted ($n > 20$) (I). Data are mean ± SEM of three biological replicates. Significant differences were determined using one-way analysis of variance (ANOVA), followed by Fisher's post hoc test (*$p < 0.05$).

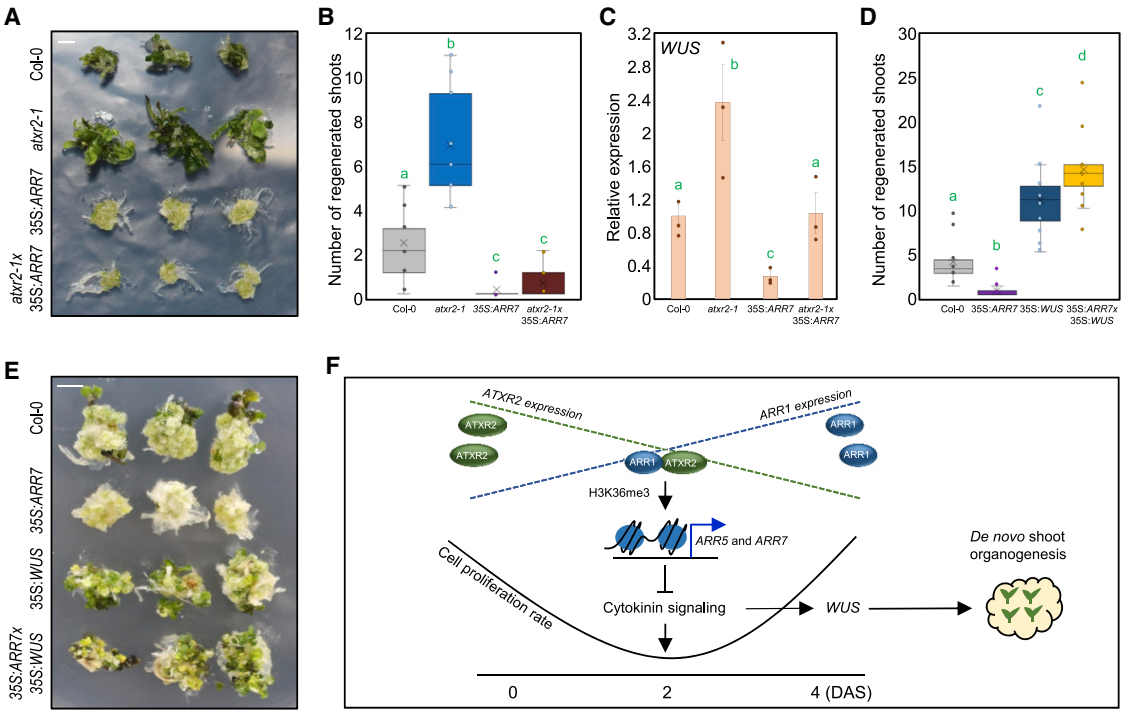

Figure 6. Type-A ARRs are epistatic to ATXR2

(A) *De novo* shoot regeneration. Calli pre-incubated on CIM for 6 days were used to induce shoot regeneration on SIM (n = 20). SIM plates were incubated under continuous light for 3 weeks and photographed. Scale bars, 5 mm.

(B) Quantification of shoot regeneration. The number of regenerated leaves derived from calli was counted (n = 20). Data indicate mean ± SEM of three biological replicates. Significant differences were determined using one-way analysis of variance (ANOVA), followed by Fisher's post hoc test. Different letters indicate significant differences (*p < 0.05).

(C) *WUS* expression in wild-type, *atxr2-1*, 35S:*ARR7*, and *atxr2-1* × 35S:*ARR7* calli. Leaf explants derived from the third and fourth leaves of 2-week-old plants were incubated on CIM for 7 days and subsequently on SIM for 6 days. Data indicate mean ± SEM of three biological replicates. Significant differences were determined using one-way ANOVA, followed by Fisher's post hoc test. Different letters indicate significant differences (*p < 0.05).

(D and E) Shoot regeneration of 35S:*ARR7* × 35S:*WUS*. Calli pre-incubated on CIM for 6 days were used to induce shoot regeneration on SIM (n = 12). The number of regenerated leaves from calli was counted (D). Data indicate mean ± SEM of three biological replicates. Significant differences were determined using one-way ANOVA, followed by Fisher's post hoc test. Different letters indicate significant differences (*p < 0.05). SIM plates incubated under continuous light for 3 weeks were photographed (E). Scale bars, 5 mm.

(F) Proposed working model showing the role of ATXR2 in balancing shoot regeneration. On SIM, the auxin-inducible *ATXR2* gene is downregulated, whereas the cytokinin-responsive *ARR1* gene is induced. Thus, ATXR2 transiently interacts with ARR1 at the early stages of shoot regeneration. The ATXR2-ARR1 complex directly binds to *ARR5* and *ARR7* promoters and catalyzes H3K36me3 deposition to activate their expression, which ultimately represses *WUS* expression. The cease in cell proliferation may ensure proper cell fate transition.

spontaneous callus formation from differentiated organs (Chanvivattana et al., 2004). Similar functions are carried out by HISTONE DEACETYLASE6 (HDA6) and HDA19 (Tanaka et al., 2008).

Upon callus formation, the root primordium identity is established on CIM, concomitant with *LBD16* and *LBD29* expression (Fan et al., 2012). The *LBD* genes are activated by the H3K9 demethylase JUMONJI C DOMAIN-CONTAINING PROTEIN30 (JMJ30), which is recruited by ARF7 and ARF19 to remove the repressive mark from *LBD16* and *LBD29* loci (Lee et al., 2018), and ATXR2, which is also recruited by ARFs and catalyzes the deposition of the active chromatin mark H3K36me3 to strengthen *LBD* expression (Lee et al., 2017). Both ATXR2 and JMJ30 act synergistically to maintain high levels of *LBD* expression in callus (Lee et al., 2018). Subsequently, the proliferating callus cells acquire pluripotency by activating the root meristem genes, such as *WOX5*, *PLT1*, and *PLT2* (Kareem et al., 2015; Sugimoto et al., 2010). HISTONE ACETYLTRANSFERASE OF THE GNAT/MYST SUPERFAMILY1 (HAG1)/GENERAL CONTROL NONREPRESSED5 (GCN5) directly activates several root meristem genes, including *WOX5*, *WOX14*, *SCARECROW* (*SCR*), *PLT1*, and *PLT2*, in the callus through the deposition of H3 acetylation marks (Kim et al., 2018).

The pluripotent callus is able to drive *de novo* shoot regeneration. WUS is a key determinant of *de novo* shoot organogenesis in callus, and extensive epigenetic reprogramming is observed at the *WUS* locus upon shoot induction (Zhang et al., 2017). Key chromatin modifications, including H3K27me3, H3K9me2, H3K4me3, and H3K9ac, exhibit extensive alterations in abundance at the early stages of incubation on SIM (He et al., 2012; Li et al., 2011), and histone modifiers including PRCs and KRYPTONITE (KYP) likely regulate histone modification at the *WUS* locus and thereby shoot regeneration (Li et al., 2011; Zhang et al.,

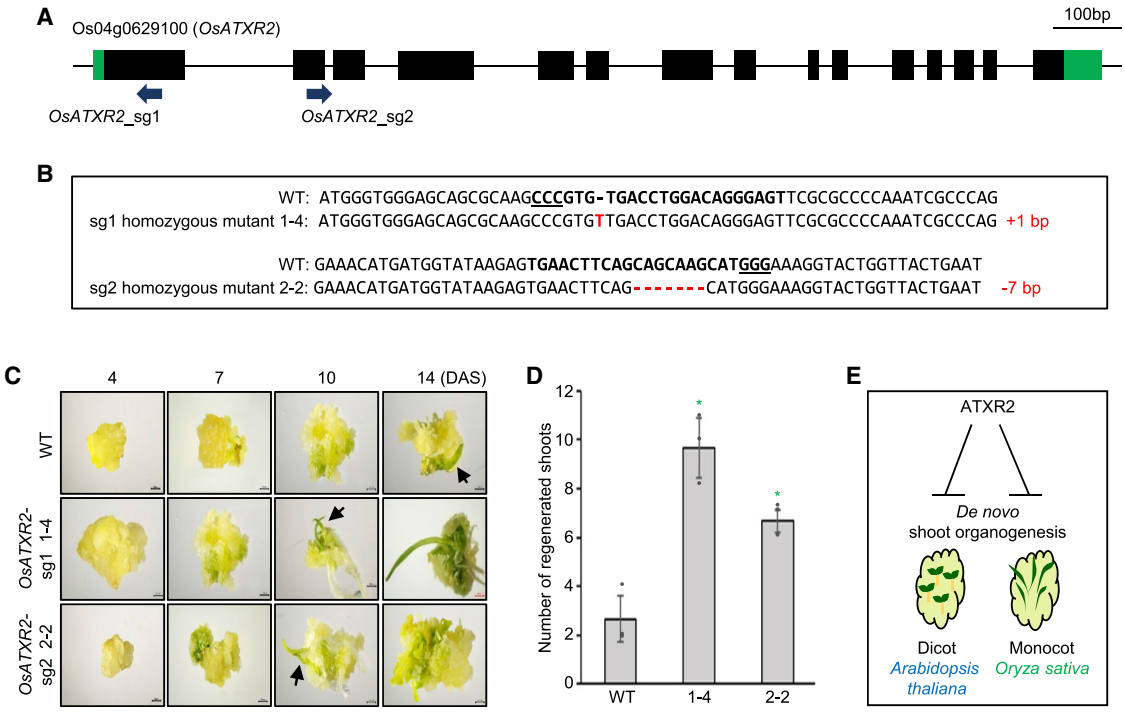

Figure 7. Functional conservation of ATXR2 in rice

(A) Schematic representation of ATXR2 homologs bearing the CRISPR-Cas9 target sites (arrows). Exons and introns are represented by black boxes and lines, respectively.

(B) CRISPR-Cas9-mediated mutagenesis. Alignment of wild-type and mutant sequences containing the CRISPR-Cas9 target sites is shown. The 20 bp single guide RNA (sgRNA) sequences adjacent to the protospacer adjacent motif (PAM) sequences (underlined) are indicated in bold in wild-type sequences. The newly created mutants contained a 1 bp insertion and 7 bp deletion.

(C and D) Comparison of shoot regeneration phenotypes including days to first-shoot emergence (arrows) from callus on SIM (C) and the number of regenerated leaves at 14 DAS (D). DAS, days after incubation on SIM. Data indicate mean ± SEM of three biological replicates. Statistically significant differences were determined using Student's t test (*$p < 0.05$).

(E) Schematic representation showing the evolutionarily conserved role of ATXR2 in repressing shoot regeneration. The *ATXR2* homologs of *Arabidopsis thaliana* (*AtATXR2*) and *Oryza sativa* (*OsATXR2*) inhibit *de novo* shoot regeneration.

2017). Additionally, changes in the DNA methylation landscape are also important for the shoot regeneration (Liu et al., 2018; Shemer et al., 2015; Zhang et al., 2017) .

Our results showed that an additional epigenetic regulatory layer balances cell fate transition during *de novo* shoot organogenesis. Type-A ARRs, which represent upstream negative regulators of *WUS*, were regulated via the ATXR2-dependent H3K36me3 deposition. During the early stages of shoot regeneration, ATXR2 bound to the *ARR5* and *ARR7* promoters and activated the expression of these genes to suppress shoot regeneration, thus ensuring a balanced cell fate transition.

Many chromatin modifiers participate in plant regeneration by regulating the epigenetic landscape, globally and/or locally, for ensuring the proper reprogramming of genetic repertoires. As low *de novo* shoot organogenesis efficiency is the main obstacle in crop transformation (Qi et al., 2014; Sabbadini et al., 2019), relevant genetic components can be used for improving the efficiency of crop transformation and regeneration. Our results show that mutations in *ATXR2* increase shoot regeneration not only in *Arabidopsis* but also in major crop plants including rice, suggesting that targeted mutagenesis of *ATXR2* homologs could be used to improve the efficiency of plant regeneration.

ATXR2 exhibits distinct roles in callus formation and shoot regeneration

Here, we demonstrate that ATXR2 performs distinct biological functions in callus formation and *de novo* shoot organogenesis. During callus formation, ATXR2 stimulates cell proliferation and establishes root primordium identity by activating *LBD* expression (Lee et al., 2017). ATXR2, along with ARF7 and ARF19, binds to *LBD16* and *LBD29* promoters and catalyzes H3K36me3 deposition to activate *LBD* gene expression during callus induction (Lee et al., 2017). The ATXR2-ARF-LBD module acts as a positive regulator of callus formation. However, at the early stage of shoot regeneration, ATXR2 performs a distinct function with a new molecular repertoire. During shoot regeneration, ATXR2 deposits the H3K36me3 mark at *ARR5* and *ARR7* loci to activate their expression. This ATXR2-mediated regulation of type-A *ARR*s is dependent on the type-B ARR1 protein during *de novo* shoot regeneration.

Interestingly, plants use distinct molecular networks involving ATXR2 for regulating callus formation and *de novo* shoot regeneration. During callus formation, the auxin-inducible ATXR2 protein regulates *LBD* gene expression, along with ARFs, to promote callus proliferation. As cytokinin-inducible type-B *ARR*s are

not expressed during callus induction, ATXR2-mediated regulation of cytokinin signaling was not apparent on CIM; the type-A *ARR* gene expression was unaffected by ATXR2 on CIM. By contrast, during shoot regeneration, type-B *ARR*s are gradually upregulated, whereas *ARF*s are repressed. ATXR2 interacts preferentially with ARR1, independent of ARFs, during shoot regeneration on SIM. These results indicate that a single histone modifier can perform different functions, depending on the interacting proteins as well as the stage of plant regeneration.

The auxin-cytokinin interaction is likely important not only for normal plant development but also for plant regeneration. For instance, during embryogenesis in wild-type plants, the endogenous auxin represses cytokinin responses by activating *ARR7* and *ARR15* expression (Müller and Sheen, 2008). In support, expression domains of *ARR7* and *ARR15* overlap with the DR5 auxin signaling reporter (Müller and Sheen, 2008), and exogenous treatment with 2,4-dichlorophenoxyacetic acid (2,4-D) expands the expression domain of *ARR7* and *ARR15* (Müller and Sheen, 2008). Lateral root and shoot development also involves auxin-cytokinin interactions. The gain-of-function mutant of *IAA17*, *axr3-3*, exhibits reduced lateral root numbers and rosette diameter (Kurepa et al., 2019), but these phenotypes are partially rescued by crossing with cytokinin-insensitive plants, such as *arr1-1* or 35S:*ARR5* (Kurepa et al., 2019). Given that ATXR2 lies at the intersection of auxin and cytokinin signaling, the ATXR2-mediated regulation of *ARR5* and *ARR7* likely underlies lateral root development, as the reduction in the number of lateral roots in *atxr2-1* was dependent on type-A ARRs (Figures S7A–S7C).

During the plant regeneration process, callus formation on CIM involves auxin metabolism and signaling, whereas *de novo* shoot organogenesis on SIM requires cytokinin signaling. Thus, auxin-cytokinin interactions are heightened at the CIM-SIM transition. Indeed, a pause in cell proliferation is frequently observed at the beginning of *de novo* shoot organogenesis on SIM (Cheng et al., 2015; Liu et al., 2018; Tamaki et al., 2009; Tian et al., 2018), which may be attributable to the auxin-cytokinin crosstalk. ATXR2 is related to a temporal reduction in cell proliferation at the initial stages of *de novo* shoot regeneration. *ATXR2* expression is increased during callus formation on CIM. However, after incubation on SIM, *ATXR2* is downregulated, whereas type-B *ARR*s are gradually upregulated. Consequently, ARR1 interacts transiently with ATXR2 and activates type-A ARRs only at the early stages of shoot regeneration, temporally inhibiting cell proliferation.

The temporal repression of cell proliferation may safeguard cell fate transition by sacrificing plant regeneration capacity caused by low cell proliferation, given that callus formed on CIM exhibits root primordium characteristics and should be converted into a new tissue type, shoot meristem, on SIM (Kareem et al., 2015; Rosspopoff et al., 2017; Sugimoto et al., 2010). Thus, the balanced cell proliferation activity at the early stages of shoot regeneration might be critical for determining the shoot regeneration rate as well as overall shoot regeneration capability. The *atxr2-1* mutant not only accelerates shoot regeneration, but also displays enhanced shoot regeneration capacity beyond levels observed in the wild-type. Taken together, ATXR2 may integrates multiple internal and external factors that affect cell fate transition, and regulates plant regeneration capability and efficiency.

Limitations of the study

In this study, we demonstrated that the auxin-inducible ATXR2 protein interacts with type-B ARR1 protein and inhibits *de novo* shoot organogenesis at the early stages of shoot regeneration on SIM through activating *type-A ARR* genes. The auxin-cytokinin interaction possibly induces a pause in cell proliferation, which may be linked to the initial specification of shoot meristem in callus. However, the impact of auxin-cytokinin interaction in cell division control needs to be confirmed. Additionally, biological relevance of temporal repression of cell division in cell fate transition should also be studied in the future.

STAR★METHODS

Detailed methods are provided in the online version of this paper and include the following:

- KEY RESOURCES TABLE
- RESOURCE AVAILABILITY
  - Lead contact
  - Materials availability
  - Data and code availability
- EXPERIMENTAL MODEL AND SUBJECT DETAILS
- METHOD DETAILS
  - RT-qPCR analysis
  - GUS staining
  - ChIP-qPCR
  - Transient expression assays using *Arabidopsis* protoplasts
  - Y2H assays
  - BiFC analysis
  - Co-IP assays
  - Immunoblot analysis
  - CRISPR sgRNA design and rice mutagenesis
- QUANTIFICATION AND STATISTICAL ANALYSIS

SUPPLEMENTAL INFORMATION

Supplemental information can be found online at https://doi.org/10.1016/j.celrep.2021.109980.

ACKNOWLEDGMENTS

This work was supported by the Basic Science Research (NRF-2020R1I1A1A01074334 to K.L.; NRF-2019R1A2C2006915 to P.J.S.) and Basic Research Laboratory (NRF-2020R1A4A2002901) programs funded by the National Research Foundation of Korea and by the Creative-Pioneering Researchers Program through Seoul National University (0409-20200281).

AUTHOR CONTRIBUTIONS

P.J.S. conceived and designed the study and wrote the manuscript. K.L., O.-S.P., J.Y.G., J.Y., and J.H.H. conducted the experiments. Y.J.J., S.B., and J.K. analyzed the data.

DECLARATION OF INTERESTS

The authors declare no competing interests.

Received: April 28, 2021
Revised: August 31, 2021
Accepted: October 20, 2021
Published: November 9, 2021

REFERENCES

Atta, R., Laurens, L., Boucheron-Dubuisson, E., Guivarc'h, A., Carnero, E., Giraudat-Pautot, V., Rech, P., and Chriqui, D. (2009). Pluripotency of *Arabidopsis* xylem pericycle underlies shoot regeneration from root and hypocotyl explants grown *in vitro*. Plant J. *57*, 626–644.

Bae, S., Park, J., and Kim, J.S. (2014). Cas-OFFinder: a fast and versatile algorithm that searches for potential off-target sites of Cas9 RNA-guided endonucleases. Bioinformatics *30*, 1473–1475.

Baumbusch, L.O., Thorstensen, T., Krauss, V., Fischer, A., Naumann, K., Assalkhou, R., Schulz, I., Reuter, G., and Aalen, R.B. (2001). The *Arabidopsis thaliana* genome contains at least 29 active genes encoding SET domain proteins that can be assigned to four evolutionarily conserved classes. Nucleic Acids Res. *29*, 4319–4333.

Buechel, S., Leibfried, A., To, J.P., Zhao, Z., Andersen, S.U., Kieber, J.J., and Lohmann, J.U. (2010). Role of A-type ARABIDOPSIS RESPONSE REGULATORS in meristem maintenance and regeneration. Eur. J. Cell Biol. *89*, 279–284.

Bustillo-Avendaño, E., Ibáñez, S., Sanz, O., Sousa Barros, J.A., Gude, I., Perianez-Rodriguez, J., Micol, J.L., Del Pozo, J.C., Moreno-Risueno, M.A., and Pérez-Pérez, J.M. (2018). Regulation of hormonal control, cell reprogramming, and patterning during *de novo* root organogenesis. Plant Physiol. *176*, 1709–1727.

Chanvivattana, Y., Bishopp, A., Schubert, D., Stock, C., Moon, Y.H., Sung, Z.R., and Goodrich, J. (2004). Interaction of Polycomb-group proteins controlling flowering in *Arabidopsis*. Development *131*, 5263–5276.

Che, P., Lall, S., and Howell, S.H. (2007). Developmental steps in acquiring competence for shoot development in *Arabidopsis* tissue culture. Planta *226*, 1183–1194.

Chen, X., Liu, X., Zhao, Y., and Zhou, D.X. (2015). Histone H3K4me3 and H3K27me3 regulatory genes control stable transmission of an epimutation in rice. Sci. Rep. *5*, 13251.

Cheng, Z.J., Wang, L., Sun, W., Zhang, Y., Zhou, C., Su, Y.H., Li, W., Sun, T.T., Zhao, X.Y., Li, X.G., et al. (2013). Pattern of auxin and cytokinin responses for shoot meristem induction results from the regulation of cytokinin biosynthesis by AUXIN RESPONSE FACTOR3. Plant Physiol. *161*, 240–251.

Cheng, Y., Liu, H., Cao, L., Wang, S., Li, Y., Zhang, Y., Jiang, W., Zhou, Y., and Wang, H. (2015). Down-regulation of multiple CDK inhibitor *ICK/KRP* genes promotes cell proliferation, callus induction and plant regeneration in *Arabidopsis*. Front. Plant Sci. *6*, 825.

Citovsky, V., Lee, L.Y., Vyas, S., Glick, E., Chen, M.H., Vainstein, A., Gafni, Y., Gelvin, S.B., and Tzfira, T. (2006). Subcellular localization of interacting proteins by bimolecular fluorescence complementation in planta. J. Mol. Biol. *362*, 1120–1131.

Dello Ioio, R., Nakamura, K., Moubayidin, L., Perilli, S., Taniguchi, M., Morita, M.T., Aoyama, T., Costantino, P., and Sabatini, S. (2008). A genetic framework for the control of cell division and differentiation in the root meristem. Science *322*, 1380–1384.

Fan, M., Xu, C., Xu, K., and Hu, Y. (2012). LATERAL ORGAN BOUNDARIES DOMAIN transcription factors direct callus formation in *Arabidopsis* regeneration. Cell Res. *22*, 1169–1180.

Galbiati, F., Sinha Roy, D., Simonini, S., Cucinotta, M., Ceccato, L., Cuesta, C., Simaskova, M., Benkova, E., Kamiuchi, Y., Aida, M., et al. (2013). An integrative model of the control of ovule primordia formation. Plant J. *76*, 446–455.

Gordon, S.P., Heisler, M.G., Reddy, G.V., Ohno, C., Das, P., and Meyerowitz, E.M. (2007). Pattern formation during *de novo* assembly of the *Arabidopsis* shoot meristem. Development *134*, 3539–3548.

Gordon, S.P., Chickarmane, V.S., Ohno, C., and Meyerowitz, E.M. (2009). Multiple feedback loops through cytokinin signaling control stem cell number within the *Arabidopsis* shoot meristem. Proc. Natl. Acad. Sci. USA *106*, 16529–16534.

He, C., Chen, X., Huang, H., and Xu, L. (2012). Reprogramming of H3K27me3 is critical for acquisition of pluripotency from cultured Arabidopsis tissues. PLoS Genet. *8*, e1002911.

Hung, F.Y., Chen, F.F., Li, C., Chen, C., Lai, Y.C., Chen, J.H., Cui, Y., and Wu, K. (2018). The *Arabidopsis* LDL1/2-HDA6 histone modification complex is functionally associated with *CCA1/LHY* in regulation of circadian clock genes. Nucleic Acids Res. *46*, 10669–10681.

Ikeda, Y., Banno, H., Niu, Q.W., Howell, S.H., and Chua, N.H. (2006). The *ENHANCER OF SHOOT REGENERATION 2* gene in *Arabidopsis* regulates *CUP-SHAPED COTYLEDON 1* at the transcriptional level and controls cotyledon development. Plant Cell Physiol. *47*, 1443–1456.

Ikeuchi, M., Sugimoto, K., and Iwase, A. (2013). Plant callus: mechanisms of induction and repression. Plant Cell *25*, 3159–3173.

Ikeuchi, M., Iwase, A., Rymen, B., Harashima, H., Shibata, M., Ohnuma, M., Breuer, C., Morao, A.K., de Lucas, M., De Veylder, L., et al. (2015). PRC2 represses dedifferentiation of mature somatic cells in *Arabidopsis*. Nat. Plants *1*, 15089.

Iwase, A., Harashima, H., Ikeuchi, M., Rymen, B., Ohnuma, M., Komaki, S., Morohashi, K., Kurata, T., Nakata, M., Ohme-Takagi, M., et al. (2017). WIND1 promotes shoot regeneration through transcriptional activation of *ENHANCER OF SHOOT REGENERATION1* in *Arabidopsis*. Plant Cell *29*, 54–69.

Jung, Y.J., Lee, H.J., Kim, J.H., Kim, D.H., Kim, H.K., Cho, Y.-G., Bae, S., and Kang, K.K. (2019). CRISPR/Cas9-targeted mutagenesis of *F3′ H, DFR* and *LDOX*, genes related to anthocyanin biosynthesis in black rice (*Oryza sativa L.*). Plant Biotechnol. Rep. *13*, 521–531.

Kamiuchi, Y., Yamamoto, K., Furutani, M., Tasaka, M., and Aida, M. (2014). The *CUC1* and *CUC2* genes promote carpel margin meristem formation during *Arabidopsis gynoecium* development. Front. Plant Sci. *5*, 165.

Kareem, A., Durgaprasad, K., Sugimoto, K., Du, Y., Pulianmackal, A.J., Trivedi, Z.B., Abhayadev, P.V., Pinon, V., Meyerowitz, E.M., Scheres, B., and Prasad, K. (2015). *PLETHORA* genes control regeneration by a two-step mechanism. Curr. Biol. *25*, 1017–1030.

Kim, H., Kim, S.T., Ryu, J., Kang, B.C., Kim, J.S., and Kim, S.G. (2017). CRISPR/Cpf1-mediated DNA-free plant genome editing. Nat. Commun. *8*, 14406.

Kim, J.Y., Yang, W., Forner, J., Lohmann, J.U., Noh, B., and Noh, Y.S. (2018). Epigenetic reprogramming by histone acetyltransferase HAG1/AtGCN5 is required for pluripotency acquisition in *Arabidopsis*. EMBO J. *37*, e98726.

Kurepa, J., Shull, T.E., and Smalle, J.A. (2019). Antagonistic activity of auxin and cytokinin in shoot and root organs. Plant Direct *3*, e00121.

Lafos, M., Kroll, P., Hohenstatt, M.L., Thorpe, F.L., Clarenz, O., and Schubert, D. (2011). Dynamic regulation of H3K27 trimethylation during *Arabidopsis* differentiation. PLoS Genet. *7*, e1002040.

Lee, H.G., and Seo, P.J. (2019). MYB96 recruits the HDA15 protein to suppress negative regulators of ABA signaling in *Arabidopsis*. Nat. Commun. *10*, 1713.

Lee, K., Park, O.S., and Seo, P.J. (2017). *Arabidopsis* ATXR2 deposits H3K36me3 at the promoters of *LBD* genes to facilitate cellular dedifferentiation. Sci. Signal. *10*, eaan0316.

Lee, K., Park, O.S., and Seo, P.J. (2018). JMJ30-mediated demethylation of H3K9me3 drives tissue identity changes to promote callus formation in *Arabidopsis*. Plant J. *95*, 961–975.

Li, W., Liu, H., Cheng, Z.J., Su, Y.H., Han, H.N., Zhang, Y., and Zhang, X.S. (2011). DNA methylation and histone modifications regulate *de novo* shoot regeneration in *Arabidopsis* by modulating *WUSCHEL* expression and auxin signaling. PLoS Genet. *7*, e1002243.

Liu, X., Kim, Y.J., Müller, R., Yumul, R.E., Liu, C., Pan, Y., Cao, X., Goodrich, J., and Chen, X. (2011). AGAMOUS terminates floral stem cell maintenance in *Arabidopsis* by directly repressing *WUSCHEL* through recruitment of Polycomb Group proteins. Plant Cell *23*, 3654–3670.

Liu, X., Chen, C.Y., Wang, K.C., Luo, M., Tai, R., Yuan, L., Zhao, M., Yang, S., Tian, G., Cui, Y., et al. (2013). PHYTOCHROME INTERACTING FACTOR3 associates with the histone deacetylase HDA15 in repression of chlorophyll biosynthesis and photosynthesis in etiolated *Arabidopsis* seedlings. Plant Cell *25*, 1258–1273.

Liu, J., Sheng, L., Xu, Y., Li, J., Yang, Z., Huang, H., and Xu, L. (2014). WOX11 and 12 are involved in the first-step cell fate transition during *de novo* root organogenesis in *Arabidopsis*. Plant Cell *26*, 1081–1093.

Liu, H., Ma, X., Han, H.N., Hao, Y.J., and Zhang, X.S. (2016). AtPRMT5 regulates shoot regeneration through mediating histone H4R3 dimethylation on *KRPs* and pre-mRNA splicing of *RKP* in *Arabidopsis*. Mol. Plant *9*, 1634–1646.

Liu, H., Zhang, H., Dong, Y.X., Hao, Y.J., and Zhang, X.S. (2018). DNA METHYLTRANSFERASE1-mediated shoot regeneration is regulated by cytokinin-induced cell cycle in *Arabidopsis*. New Phytol. *217*, 219–232.

Liu, Y., Zhou, C., Huang, S., Dang, L., Wei, Y., He, J., Zhou, Y., Mao, S., Tao, W., Zhang, Y., et al. (2020a). A Cas-embedding strategy for minimizing off-target effects of DNA base. Nat. Commun. *11*, 6073.

Liu, Z., Dai, X., Li, J., Liu, N., Liu, X., Li, S., and Xiang, F. (2020b). The type-B cytokinin response regulator ARR1 inhibits shoot regeneration in an ARR12-dependent manner in *Arabidopsis*. Plant Cell *32*, 2271–2291.

Lu, Y., Ye, X., Guo, R., Huang, J., Wang, W., Tang, J., Tan, L., Zhu, J.K., Chu, C., and Qian, Y. (2017). Genome-wide targeted mutagenesis in rice using the CRISPR/Cas9 system. Mol. Plant *10*, 1242–1245.

Matsuo, N., Makino, M., and Banno, H. (2011). *Arabidopsis* ENHANCER OF SHOOT REGENERATION (ESR)1 and ESR2 regulate *in vitro* shoot regeneration and their expressions are differentially regulated. Plant Sci. *181*, 39–46.

Moubayidin, L., Di Mambro, R., and Sabatini, S. (2009). Cytokinin-auxin crosstalk. Trends Plant Sci. *14*, 557–562.

Müller, B., and Sheen, J. (2008). Cytokinin and auxin interaction in root stem-cell specification during early embryogenesis. Nature *453*, 1094–1097.

Park, J., Bae, S., and Kim, J.S. (2015). Cas-Designer: a web-based tool for choice of CRISPR-Cas9 target sites. Bioinformatics *31*, 4014–4016.

Qi, W., Tinnenbroek-Capel, I.E., Schaart, J.G., Huang, B., Cheng, J., Visser, R.G., Van Loo, E.N., and Krens, F.A. (2014). Regeneration and transformation of *Crambe abyssinica*. BMC Plant Biol. *14*, 235.

Rosspopoff, O., Chelysheva, L., Saffar, J., Lecorgne, L., Gey, D., Caillieux, E., Colot, V., Roudier, F., Hilson, P., Berthomé, R., et al. (2017). Direct conversion of root primordium into shoot meristem relies on timing of stem cell niche development. Development *144*, 1187–1200.

Ryu, H., Cho, H., Bae, W., and Hwang, I. (2014). Control of early seedling development by BES1/TPL/HDA19-mediated epigenetic regulation of *ABI3*. Nat. Commun. *5*, 4138.

Sabbadini, S., Capriotti, L., Molesini, B., Pandolfini, T., Navacchi, O., Limera, C., Ricci, A., and Mezzetti, B. (2019). Comparison of regeneration capacity and Agrobacterium-mediated cell transformation efficiency of different cultivars and rootstocks of *Vitis spp.* via organogenesis. Sci. Rep. *9*, 582.

Salvi, E., Rutten, J.P., Di Mambro, R., Polverari, L., Licursi, V., Negri, R., Dello Ioio, R., Sabatini, S., and Ten Tusscher, K. (2020). A self-organized PLT/Auxin/ARR-B network controls the dynamics of root zonation development in *Arabidopsis thaliana*. Dev. Cell *53*, 431–443.e23.

Shemer, O., Landau, U., Candela, H., Zemach, A., and Eshed Williams, L. (2015). Competency for shoot regeneration from *Arabidopsis* root explants is regulated by DNA methylation. Plant Sci. *238*, 251–261.

Sugimoto, K., Jiao, Y., and Meyerowitz, E.M. (2010). *Arabidopsis* regeneration from multiple tissues occurs via a root development pathway. Dev. Cell *18*, 463–471.

Tamaki, H., Konishi, M., Daimon, Y., Aida, M., Tasaka, M., and Sugiyama, M. (2009). Identification of novel meristem factors involved in shoot regeneration through the analysis of temperature-sensitive mutants of *Arabidopsis*. Plant J. *57*, 1027–1039.

Tanaka, M., Kikuchi, A., and Kamada, H. (2008). The *Arabidopsis* histone deacetylases HDA6 and HDA19 contribute to the repression of embryonic properties after germination. Plant Physiol. *146*, 149–161.

Tian, X., Zhang, C., and Xu, J. (2018). Control of cell fate reprogramming towards *de novo* shoot organogenesis. Plant Cell Physiol. *59*, 708–714.

To, J.P., Deruère, J., Maxwell, B.B., Morris, V.F., Hutchison, C.E., Ferreira, F.J., Schaller, G.E., and Kieber, J.J. (2007). Cytokinin regulates type-A *Arabidopsis* Response Regulator activity and protein stability via two-component phosphorelay. Plant Cell *19*, 3901–3914.

Tomlinson, L., Yang, Y., Emenecker, R., Smoker, M., Taylor, J., Perkins, S., Smith, J., MacLean, D., Olszewski, N.E., and Jones, J.D.G. (2019). Using CRISPR/Cas9 genome editing in tomato to create a gibberellin-responsive dominant dwarf *DELLA* allele. Plant Biotechnol. J. *17*, 132–140.

Xie, M., Chen, H., Huang, L., O'Neil, R.C., Shokhirev, M.N., and Ecker, J.R. (2018). A B-ARR-mediated cytokinin transcriptional network directs hormone cross-regulation and shoot development. Nat. Commun. *9*, 1604.

Yamaguchi, N., Winter, C.M., Wellmer, F., and Wagner, D. (2015). Identification of direct targets of plant transcription factors using the GR fusion technique. Methods Mol. Biol. *1284*, 123–138.

Zhang, T.Q., Lian, H., Zhou, C.M., Xu, L., Jiao, Y., and Wang, J.W. (2017). A two-step model for de novo activation of *WUSCHEL* during plant shoot regeneration. Plant Cell *29*, 1073–1087.

Zubo, Y.O., Blakley, I.C., Yamburenko, M.V., Worthen, J.M., Street, I.H., Franco-Zorrilla, J.M., Zhang, W., Hill, K., Raines, T., Solano, R., et al. (2017). Cytokinin induces genome-wide binding of the type-B response regulator ARR10 to regulate growth and development in *Arabidopsis*. Proc. Natl. Acad. Sci. U S A *114*, E5995–E6004.

STAR★METHODS

KEY RESOURCES TABLE

REAGENT or RESOURCE	SOURCE	IDENTIFIER
Antibodies		
anti-MYC	Millipore	Cat#05-724; RRID:AB_568800
anti-GFP	Abcam	Cat#ab290; RRID:AB_303395
anti-H3K4me3	Millipore	Cat#07-473; RRID:AB_1977252
anti-H3K36me3	Abcam	Cat#ab9050; RRID:AB_306966
anti-Rabbit IgG-HRP	Santa Cruz	Cat#sc-2357; RRID:AB_628497
anti-m-IgGκ BP-HRP	Santa Cruz	Cat#SC-516102; RRID:AB_2687626
Bacterial and virus strains		
Escherichia coli strain DH5a	Enzynomics	Cat#CP010
Agrobacterium strain GV3101	Lab stock	N/A
Agrobacterium-tumefaciens strain EHA105	Lab stock	N/A
Yeast strain AH109	Clontech	N/A
Chemicals, peptides, and recombinant proteins		
Indole-3-Acetic acid	Duchefa	Cat#I0901
2,4-DICHLOROPHENOXYACETIC ACID	Duchefa	Cat#D0911
2-isopentenyladenine	Sigma-Aldrich	Cat#D7674
Kinetin	Duchefa	Cat#K0905
6-Benzylaminopurine	Duchefa	Cat#B0904
Dexamethasone	Sigma-Aldrich	Cat#D1756
X-Gluc	GoldBio	Cat#G1281C
4-methylumbelliferyl-beta-D-glucuronide	Millipore	Cat#474427
DNA/protein-A agarose beads	Millipore	Cat#16-157
DNA/protein-A/G agarose beads	Santa Cruz	Cat#SC-2003
TransZol Up	Transgen Biotech	Cat#ET111-01
Critical commercial assays		
Luciferase assay system kit	Promega	Cat#E1500
qPCR PreMix (SYBR Green)	Enzynomics	Cat#RT501M
MMLV Reverse Transcriptase	MGmed	Cat#MR01601
Experimental models: organisms		
Arabidopsis thaliana line Col-0	NASC	N1093
Arabidopsis thaliana line *atxr2-1*	ABRC	SAIL_600_E07
Arabidopsis thaliana line *arr1-3*	ABRC	CS6971
Arabidopsis thaliana line *arr10-5*	ABRC	SALK_098604
Arabidopsis thaliana line *arr12-1*	ABRC	CS6978
Arabidopsis thaliana line *arf7-1xarf19-2*	ABRC	CS24630
Arabidopsis thaliana line *ARR1-C1xYpet*	ABRC	CS71599
Arabidopsis thaliana line 35S:*ARR1-MYC*	This study	N/A
Arabidopsis thaliana line 35S:*ARR7*	This study	N/A
Arabidopsis thaliana line 35S:*ARR5*	This study	N/A
Arabidopsis thaliana line 35S:*WUS*	This study	N/A
Arabidopsis thaliana line 35S:*MYC-ATXR2*	This study	N/A
Arabidopsis thaliana line *35S:ATXR2-GR*	This study	N/A
Arabidopsis thaliana line *pATXR2::GUS*	This study	N/A

(*Continued on next page*)

Continued

REAGENT or RESOURCE	SOURCE	IDENTIFIER
Oryza sativa line *OsATXR2-sg1 1-4*	This study	N/A
Oryza sativa line *OsATXR2-sg2 2-2*	This study	N/A
Oligonucleotides		
Primers used are shown in Tables S1, S2, and S3	This study	N/A
Recombinant DNA		
pBA002a-GUS-ATXR2	This study	N/A
MYC-pBA-ATXR2	This study	N/A
MYC-pBA-ARR1	This study	N/A
JJ461-ATXR2	This study	N/A
pGBKT7-ATXR2	This study	N/A
pGADT7-ARR1	This study	N/A
pGADT7-ARR10	This study	N/A
pGADT7-ARR12	This study	N/A
E3081-ATXR2	This study	N/A
E3082-ARR1	This study	N/A
Modified pCAMBIA1305-ARR5	This study	N/A
Modified pCAMBIA1305-ARR7	This study	N/A
GR modified pEarlyGate 100-ATXR2	This study	N/A
pBOsC-OsATXR2_sg1	This study	N/A
pBOsC-OsATXR2_sg1	This study	N/A

RESOURCE AVAILABILITY

Lead contact

Further information and requests for resources and reagents should be directed to the Lead Contact, Pil Joon Seo (pjseo1@snu.ac.kr).

Materials availability

All materials generated in this study are available from the Lead Contact.

Data and code availability

- All data reported in this paper will be shared by the lead contact upon request.
- This paper does not report original code.
- Any additional information required to reanalyze the data reported in this paper is available from the lead contact upon request.

EXPERIMENTAL MODEL AND SUBJECT DETAILS

Arabidopsis thaliana ecotype Columbia (Col-0) was used for all experiments, unless specified otherwise. Plants were grown under long-day (LD) conditions (16 h light/8 h dark cycles) using white fluorescent lamps (150 μmol photons $m^{-2}s^{-1}$) at 22–23°C. To induce callus formation, leaf explants harvested from 2-week-old plants were placed on CIM (B5 medium supplemented with 0.5 μg/ml 2,4-D and 0.05 μg/ml kinetin), followed by incubation in the dark at 22°C for 6–7 days. To induce shoot regeneration, calli pre-incubated on CIM for 6–7 days were transferred to SIM (B5 medium supplemented with 0.9 μmol/L indole-3-acetic acid [IAA] and 2.5 μmol/L 2-isopentenyladenine [2-iP]), followed by incubation at 25°C under continuous light.

To examine the effects of hormones on *ATXR2* expression, 2-week-old plants grown on Murashige and Skoog (MS) medium supplemented with agar were transferred to liquid MS medium supplemented with 1 μM IAA or 1 μM 6-benzylaminopurine (6-BAP), and incubated for 24 h. To examine the effect of wounding, the third and fourth leaves of 2-week-old seedlings were excised and placed on hormone-free MS medium for 24 h. To conduct DEX treatment, leaf explants from the third and fourth leaves of 2-week-old 35S:*ATXR2-GR* plants were incubated on CIM for 7 days and subsequently on SIM for 4 days.

METHOD DETAILS

RT-qPCR analysis

Total RNA was extracted from the plant materials of interest using the TransZol Up (Transgen Biotech), according to the manufacturer's instructions. First-strand cDNA was synthesized from 2 μg of total RNA using Moloney Murine Leukemia Virus reverse transcriptase (MGmed) and dT20 oligo. The cDNA was diluted to a volume of 100 μL with Tris-EDTA (TE) buffer, and 1 μL of the diluted cDNA was used for RT-qPCR.

The RT-qPCR reactions were performed in 96-well plates using the StepOnePlus Real-Time PCR System (Applied Biosystems). Gene expression levels were normalized relative to the expression level of the *EUKARYOTIC TRANSLATION INITIATION FACTOR 4A1* (*eIF4A*) gene (At3g13920). PCR primers used for RT-qPCR are listed in Table S1. Relative gene expression levels were quantified using the comparative ΔΔCt method. The threshold cycle (Ct) for each reaction was determined automatically with the analysis software using default parameters (Applied Biosystems). The specificity of RT-qPCR reactions was determined by melting curve analysis.

GUS staining

To perform histochemical staining of GUS activity, plant materials were fixed by immersing in 90% (v/v) acetone for 20 min on ice, and then washed twice with rinsing solution (50 mM sodium phosphate [pH 7], 0.5 mM potassium ferricyanide [$K_3Fe(CN)_6$], and 0.5 mM potassium ferrocyanide [$K_4Fe(CN)_6$]). Subsequently, the fixed samples were incubated in staining solution containing 2 mM 5-bromo-4-chloro-3-indolyl-β-d-glucuronide (X-Gluc; Duchefa) at 37°C for 24 h.

ChIP-qPCR

The harvested plant materials were cross-linked with 1% formaldehyde. The fixed samples were ground to a fine powder in liquid nitrogen and then sonicated. The sonicated chromatin complexes were precipitated with salmon sperm DNA/protein-A (16-157; Millipore) or DNA/protein-A/G agarose beads (SC-2003; Santa Cruz) and then incubated with anti-MYC (05-724; Millipore), anti-H3K4me3 (07-473; Millipore), and anti-H3K36me3 (ab9050; Abcam) antibodies. The precipitated DNA was purified using phenol/chloroform/isoamyl alcohol and sodium acetate (pH 5.2). The abundance of specific DNA fragments in the precipitate was quantified by qPCR, and values were normalized relative to the *eIF4a* gene. The levels of precipitated DNA fragments were quantified by qPCR using sequence-specific primer sets (Table S2).

Transient expression assays using *Arabidopsis* protoplasts

To conduct transient expression assays, reporter and effector plasmids were constructed as follows. To construct reporter plasmids, ~1,500 bp sequence of the *ARR5* and *ARR7* promoters was cloned separately into the modified pCAMBIA1305 vector, which contained a minimal cauliflower mosaic virus (CaMV) 35S promoter and the *β-glucuronidase* (*GUS*) gene. To construct effector plasmids, cDNAs of *ARR1* and *ATXR2* were individually cloned into the pBA002 vector containing the CaMV 35S promoter.

To isolate *Arabidopsis* protoplasts, the fifth leaf was harvested from *Arabidopsis* plants and cut into 0.5 mm strips using a clean razor blade. The leaf strips were incubated in an enzyme solution containing 1% (w/v) cellulose RS, 0.1% (w/v) macerozyme R10 (Karlan Biochemicals, Cottonwood, AZ, USA), 0.6 M mannitol, 10 mM MES (pH 5.7), 1 mM $CaCl_2$, 1 mM $MgCl_2$, 10 mM β-mercaptoethanol, and 0.1% bovine serum albumin (w/v), and were digested by gentle shaking at room temperature for 3 h. The enzyme solution was sieved through a 70 μm nylon mesh (Carolina Biologicals, Burlington, NC, USA) and spun at 45 × *g* for 5 min. The pellet was washed twice and re-suspended in wash solution (0.6 M mannitol and 4 mM MES; pH 5.7). The recombinant reporter and effector plasmids were co-transformed into *Arabidopsis* protoplasts by polyethylene glycol (PEG)-mediated transformation. Another plasmid carrying the *luciferase* gene under the control of the CaMV 35S promoter was also co-transformed into *Arabidopsis* protoplasts, along with the reporter and effector plasmids, as an internal control. The transformed protoplasts were incubated in the dark at 23°C. After incubation for 16 h, GUS activity was quantified, and luciferase assay was performed using the Luciferase Assay System Kit (Promega, Madison, WI, USA).

Y2H assays

Y2H assays were performed using the BD Matchmaker system (Clontech). Full-length or truncated cDNA of *ARR1* was cloned into the pGADT7 vector to generate the *pGADT7-ARR1-GAL4-AD* construct. Additionally, full-length cDNA of *ATXR2* was cloned into the pGBKT7 vector to generate the *pGBKT7-ATXR2-GAL4-BD* construct. Full length GAL4 transcription factor was expressed as a positive control (Clontech). The expression constructs were co-transformed into yeast (*Saccharomyces cerevisiae*) strain AH109 harboring the *LacZ* and *histidine* (*His*) reporter genes. The transformed yeast cells were selected by growth on synthetic defined (SD) medium lacking leucine and tryptophan (SD/-Leu/-Trp) and on SD medium lacking Leu, Trp, His, and adenine (SD/-Leu/-Trp/-His/-Ade).

BiFC analysis

Full-length *ATXR2* and *ARR1* coding sequences were fused in-frame to the 5′ end of a gene sequence encoding the N-terminal half of EYFP in the pSATN-nEYFP-C1 vector (E3081) or the C-terminal half of EYFP in the pSATN-cEYFP-C1 vector (E3082)

(Citovsky et al., 2006). The mCherry construct was used as a nucleus localization marker. The recombinant constructs were co-transfected into *Arabidopsis* mesophyll protoplasts by the PEG-calcium transfection method. Transformed protoplasts were incubated at 23 °C for 12–16 h in darkness, and fluorescence emitted by these protoplasts was monitored using the CQ1 confocal microscope (Yokogawa, Japan).

Co-IP assays

To perform Co-IP assays, 35S:*ATXR2-GFP* transgenic plants were crossed with 35S:*ARR1-MYC* transgenic plants. Two-week-old *Arabidopsis* seedlings were homogenized in liquid nitrogen, and total protein extracts were prepared in protein extraction buffer (25 mM Tris-HCl [pH 7.5], 150 mM NaCl, 5% glycerol, 0.05% Nonidet P-40, 2.5 mM EDTA, 1 mM phenylmethylsulfonyl fluoride [PMSF], and 1 × protease inhibitor cocktail). Five percent of the extracts were reserved for use as input (control). The remaining protein extracts were mixed with anti-MYC antibody (05-724, 1:500 dilution; Millipore), coupled to DNA/protein-A/G agarose beads (SC-2003; Santa Cruz), and incubated at 4°C for 24 h. The precipitated samples were washed at least four times with protein extraction buffer and then eluted using 1 × sodium dodecyl sulfate (SDS) loading buffer. The samples were subjected to SDS–polyacrylamide gel electrophoresis (PAGE), and recombinant proteins were detected using anti-MYC antibody (05-724; Millipore) or anti-GFP antibody (ab290; Abcam).

Immunoblot analysis

The harvested plant materials were ground in liquid nitrogen, and total cellular extracts were suspended in SDS–PAGE sample loading buffer. The protein samples were then loaded onto a 10% polyacrylamide gel and separated by SDS–PAGE. Protein samples in the gel were blotted onto Hybond-P+ membranes (Amersham Pharmacia). Epitope-tagged proteins were immunologically detected using specific antibodies.

CRISPR sgRNA design and rice mutagenesis

CRISPR-Cas9 sgRNA targets within *OsATXR2* coding sequence were selected using Cas-OFFinder (http://www.rgenome.net/cas-offinder) and Cas-Designer (http://www.rgenome.net/cas-designer) (Park et al., 2015), web-based softwares. Each target sequence was cloned into a CRISPR-Cas9 binary vector for monocot, pBOsC, and the constructs were transformed into calli by *Agrobacterium-tumefaciens* strain EHA105, according to the previously reported method (Jung et al., 2019). Transgenic plants were regenerated and T-DNA insertion was confirmed by PCR analysis using Bar gene-specific primers. Among the transformants, CRISPR-edited mutant lines were selected by targeted deep sequencing analysis. To analyze mutations generated by Cas9, genomic DNA was extracted from individual rice plants. DNA segment that contains each Cas9 target site were amplified with PCR using pair of primer (Table S3). Amplicon library was subjected to paired-end read sequencing using Illumina Miniseq. Obtained data were analyzed using Cas-Analyzer (http://www.rgenome.net/cas-analyzer/#!). Reads that occurred only once were excluded to remove errors associated with PCR and sequencing. Indel mutations located around the Cas9 cleavage site (3 bp upstream of the protospacer adjacent motifs sequence) were considered as mutations induced by Cas9.

QUANTIFICATION AND STATISTICAL ANALYSIS

Data for quantification analyses are presented as mean ± standard error of mean (SEM). Statistical analyses were performed using Prism (GraphPad). Number of replicates is shown in the figure legends. The data were subjected to statistical analysis using either Student's t test or One-way ANOVA analysis with Fisher's post hoc test as specified in individual figure legends.